Science
AAAS

Supplementary Materials for

Error-prone, stress-induced 3′ flap–based Okazaki fragment maturation supports cell survival

Haitao Sun *et al.*

Corresponding authors: Li Zheng, lzheng@coh.org; Binghui Shen, bshen@coh.org

Science **374**, 1252 (2021)
DOI: 10.1126/science.abj1013

The PDF file includes:

Other Supplementary Material for this manuscript includes the following:

Materials and Methods

Yeast strains and plasmids

All yeast strains (see Table S4 for sources) used for genetic studies were derivatives of three *Saccharomyces cerevisiae* yeast strains: the WT control strain (RDKY2672: *MATa, his3Δ200, ura3-52, leu2Δ1, trp1Δ63, ade2Δ1, ade8, hom3-10, lys2ΔBgl;* RDKY2669: *MATα, his3Δ200, ura3-52, leu2Δ1, trp1Δ63, ade2Δ1, ade8, hom3-10, lys2ΔBgl*), the *rad27Δ* strain (RDKY2608: *MATa, his3Δ200, ura3-52, leu2Δ1, trp1Δ63, ade2Δ1, ade8, hom3-10, lys2ΔBgl, rad27Δ::URA3*) (*12*), and *dna2-1* mutant strain, which carries the nuclease abolishing P504S *dna2* mutation (4×154-9A: *MATa, his3Δ200, leu2Δ1, trp1*-289). All derived yeast strains are listed in Table S4. The genotypes of these yeast strains were verified using PCR-based genotyping. The *pol3* knock-in mutant yeast strain was generated using a previously published two-step approach for knock-in of point mutations in yeast (*25*). A PCR-amplified DNA fragment encoding the Pol3 mutation and the selection marker *HIS3* was transfected into *rad27Δ* yeast cells. Stably transfected cells, as indicated by growth on synthetic complete (SC)-His nutrient-deficient plates, were selected and knock-in of the *pol3* mutation was confirmed by PCR-based Sanger DNA sequencing. The *rad27Δ* or *rad27Δ pol3* ITD knock-in yeast cells were transfected with a PCR-amplified DNA fragment encoding the Flag tag and the hygromycin B selection marker. The PCR fragment was also flanked by two 39 bp fragments (Upstream: 5' AAAGAGCTGCAGGAGAAAGTAGAACAATTAAGCAAATGG 3', Downstream: 5' TATCTATTTATATATACATATATATCCACCAACATGCAA 3'), corresponding to the C-terminus and 3'UTR of the *POL3* gene. Flag-tagged Pol3 colonies were selected in yeast extract peptone dextrose (YPD) medium containing hygromycin B. Expression of Flag-tagged WT or ITD Pol3 in WT or *rad27Δ* was verified by western blot analysis using the anti-Flag tag antibody (Cat# F1804-200UG, SIGMA).

DUN1 or SML1 gene knock-out cells were constructed using a recombination-based approach. WT or *rad27Δ* yeast cells were transfected with a PCR-amplified DNA fragment containing the *HIS3 or TRP1* gene, which was flanked by two 39 bp fragments (*DUN1* upstream: 5' TAGTCGAGAGTAACAAGTAAAGGGGCTTAACATACAGTA 3', *DUN1* downstream: 5' TGCATGTTGGTGGATATATATGTATATATAAATAGATAC 3', *SML1* upstream: 5' CTCACTAACCTCTCTTCAACTGCTCAATAATTTCCCGCT3', *SML1* downstream: 5' GGAAATGGAAAGAGAAAAGAAAAGAGTATGAAAGGAACT3'), corresponding to the 5' or the 3'end of the *DUN1 or SML1* gene, respectively, for recombination. Knock-out of *DUN1 or SML1* (*dun1Δ or sml1Δ*) in the transformant colonies, which were selected in SC-His or SC-Trp growth medium, was verified using PCR-based Sanger DNA sequencing. The protease-deficient *S. cerevisiae* yeast strain YRP654 (a gift of Dr. Satya Prakash) was used to express Polδ and Polδ-ITD mutant complexes.

Genetic crosses

Previous studies showed synthetic lethality of *rad27Δ* with *exo1Δ* or of *rad27Δ* with the nuclease activity-abolishing *dna2* mutation P504S (*dna2-1* mutant allele) (*26, 27*). To assess if

double mutation of *rad27*Δ and *pol3* ITD could rescue this synthetic lethality at 30ºC, diploid yeast mutant cells were created by genetic crosses of the *rad27*Δ::*LEU2 pol3* ITD::*HIS3* mutant strain with the *exo1*Δ::*URA3* strain or with the *dna2-1* strain. Ascospores from the diploid mutant cells were isolated as previously described (*28, 29*). The haploids, carrying either the MATa or the MATα allele, were confirmed by PCR analysis using the primers: MATa forward primer: 5' ACTCCACTTCAAGTAAGAGTTTG 3', MATα forward primer: 5' GCACGGAATATGGGACTACTTCG 3', and MAT reverse primer: 5' AGTCACATCAAGATCGTTTATGG 3'. The isolated spores germinated and grew into colonies on nutrient-deficient medium plates to select spores that carried a specific combination of mutant alleles (Table S2, S3). In genetic crosses of the *rad27*Δ::*LEU2 pol3* ITD::*HIS3* strain with the *exo1*Δ::*URA3* strain, the viability of spores carrying the *rad27*Δ::*LEU2 pol3* ITD::*HIS3* and *exo1*Δ::*URA3* alleles were assessed by the capacity to grow and form colonies on SC-Leu-His-Ura plates, which selected for *rad27*Δ *pol3* ITD *exo1*Δ cells. In genetic crosses of the *rad27*Δ::*LEU2 pol3* ITD::*HIS3* strain with the *dna2-1* strain, which has no linked selection marker, the presence of viable spores carrying *rad27*Δ::*LEU2 pol3* ITD::*HIS3 dna2-1* alleles was determined using PCR-based DNA sequencing of the *DNA2* allele from independent colonies formed on SC-Leu-His plates, which selected for *rad27*Δ *pol3* ITD cells.

Canavanine resistance assays

Canavanine resistance (Can^r) assays were used to measure mutation rates and mutation spectra. The Can^r-based forward mutation rate in the yeast strains was determined as previously described (*12, 30*). Briefly, single colonies (*n*=10) were picked and cultured in YPD medium overnight at 30°C. For restrictive temperature stress conditions, yeast cells were transferred into fresh medium and incubated at 37°C for 4 h. Cells from each independent colony were then diluted into sterile water and plated onto YPD plates or plates with arginine-deficient selective medium containing 60 µg/mL canavanine (Sigma-Aldrich, C9758). Numbers of Can^r colonies were counted and the data were analyzed using the method of Lea and Coulson (*31*). In this method, the average number of Can^r mutations per culture M is calculated based on the equation: $r0 = M (1.24 + \ln M)$, in which r0 is the median number of Can^r colony-forming units per culture. The mutation rate is calculated using the equation $r = M/N$, where N is the average number of viable cells per plating. To define the mutation spectra of the yeast strains, ~20 single Can^r colonies were picked from canavanine plates (one colony was picked per plate) and grown in YPD medium. The total genomic DNA was extracted and purified. The CAN1 gene was PCR-amplified for each Can^r colony and CAN1 gene mutations were detected using Sanger sequencing.

Generation of revertant lines

To produce *rad27*Δ revertants for mutation analysis, a single *rad27*Δ colony was cultured in YPD medium at 30°C. The cultured cells were then diluted into fresh YPD medium and incubated at 37°C. Cells were diluted into fresh YPD medium every 4 days for 20 days. The cells were then plated onto YPD plates and incubated at 37°C for 48 h. Any viable colonies were considered revertants. The revertant phenotype was verified by conducting spot assays at various

temperatures. Briefly, yeast cells [optical density (OD_{600}) = ~0.4] of the indicated genetic backgrounds were serially diluted at a 1:5 ratio. The diluted cells were spotted onto YPD plates, and incubated at 30℃ (optimal temperature), 25℃ (sub-optimal temperature), or 37℃ (restrictive temperature) for 48 h.

To evaluate the revertant frequency, *rad27*Δ or *rad27*Δ *dun1*Δ cells from a single colony were cultured in YPD medium overnight at 30℃. The same number of yeast cells (0.1–1 million; quantified by hemacytometer) was then cultured in fresh YPD and incubated at 37℃ for 0, 2, 4, 8, or 24 h (*n*=3). The cell culture was then plated onto YPD plates and incubated at 37℃ for 48 h. The number of colonies was scored and the revertant frequency (%) was calculated by dividing the number of colonies by the number of viable cells before incubation at 37℃.

MMS sensitivity assay

To assay the MMS sensitivity of different yeast strains, 0.005%, 0.01%, 0.015% or 0.02% MMS was added to YPD plates after autoclaving, and plates were used the same day. Yeast cells were serially diluted and spotted on YPD plates containing different levels of MMS. The plates were incubated at 30℃ for 48 h.

Animal studies

FEN1 F343A/F344A (FFAA) heterozygous mice (WT/FFAA, 129S1 genetic background), which develop lung adenoma or adenocarcinoma at a high frequency (*32*), were in-line bred and housed in the Animal Resource Center at City of Hope. All experimental protocols involving animals were approved by the Institutional Animal Care and Use Committee of City of Hope in compliance with the Public Health Service policies of the United States. To determine the extent to which inhibiting Chk1 suppressed cancer development in FEN1 FFAA mutant mice, randomly selected WT or WT/FFAA male or female mice (6 months old) were treated with 0.025 mg/kg body weight SB218078 (Chk1 inhibitor) in DMSO via intraperitoneal injection once per week for four weeks. Untreated control mice were injected with the same volume of DMSO (vehicle). All mice were euthanized at 16 months of age. The presence of lung tumors was determined using anatomic and histopathological analysis in blinding fashion. For whole exome sequencing (WES) studies, WT or FEN1 A159V/WT mice (*33*) were euthanized at 16 months, and normal lung or lung tumors were dissected for total genomic DNA extraction and purification.

Protein expression and purification

Recombinant Pol3, Pol31, and Pol32 were co-expressed in yeast cells and purification of the Polδ complex was performed as described previously (*34-36*). All of the following purification steps were performed at 4℃. Briefly, ~10 g of frozen yeast cells expressing WT Polδ (Pol3, Pol31, and Pol32 subunits) or Polδ-ITD (*pol3* ITD, Pol31, and Pol32 subunits) were re-suspended in 3 volumes of 1 × CBB (50 mM Tris–HCl, pH 7.5, 10% sucrose, 1 mM EDTA) containing 500 mM NaCl and protease inhibitor cocktail (Thermo Scientific, 78429) and then

disrupted in a Bullet Blender Gold (Next Advance, Inc) with cooling (dry ice). Cell debris was removed by centrifugation (20,000 × g, 10 min), after which the clarified whole cell extract was prepared by further centrifugation (20,000 × g, 120 min). Ammonium sulfate (0.28 g/mL) was added to the whole cell extract to precipitate the proteins. The resulting pellet was re-suspended in 10 mL of 1 × GBB (50 mM Tris–HCl, pH 7.5, 10% glycerol, 1 mM EDTA) containing 200 mM NaCl (GBB200) and protease inhibitor cocktail and dialyzed overnight against 100 volumes of 1 × GBB. The dialyzed sample was then passed slowly over a 2-mL Glutathione Sepharose 4B column (GE Healthcare, 17-0756-01), washed with 10 volumes of 1 × GBB250, and equilibrated in 1 × GBB150. Proteins were eluted by incubation with 1 × GBB150 containing 40 mM glutathione and 0.01% Nonidet P-40 and subsequently mixed with 0.5 mL anti-FLAG M2 agarose (Sigma-Aldrich, A2220) and rocked overnight, washed with 1 × GBB250, and equilibrated in 1 × GBB150 containing 0.01% Nonidet P-40. The Polδ proteins were eluted by treatment with 20 units of PreScission protease (GE Healthcare, GE27-0843-01) overnight at 4°C. The eluted recombinant Polδ protein was then incubated with 100 μL of Glutathione Sepharose 4B to remove residual PreScission protease and GST-tag. The purity of the final Polδ complex was evaluated using SDS-PAGE (fig. S20A).

Recombinant 6His-tagged yeast DNA Lig I (Cdc9) or PCNA (Pol30) was expressed in the *E. coli* strain BL21 (DE3) and purified using Ni^{++}-NTA agarose as previously described (*37*). The 6His-tagged DNA Lig I was further purified using heparin chromatography. Protein bound to the heparin column was eluted using a linear gradient of 50–500 mM KCl in buffer containing 20 mM K-PO_4, pH 7.5, 0.1 mM EDTA, and 10% glycerol. The eluted peak fraction was subjected to buffer exchange with storage buffer (10 mM Tris-HCl, pH7.5, 50 mM NaCl, 10% glycerol) and concentrated using a centrifugal filter unit. The purity of the final Lig I or PCNA protein was evaluated using SDS-PAGE (fig. S20B, S20C).

Nuclease and polymerase activity and reconstitution assays

The nuclease and polymerase activities of WT yeast Polδ and Polδ-ITD were assayed using 5' ^{32}P-labeled DNA substrates, which were prepared as previously described (*38*). The 5' ^{32}P-labeled DNA substrates for primer extension or strand displacement DNA synthesis were prepared using the synthetic oligonucleotides listed in Tables S5 and S6. Purified recombinant WT Polδ or Polδ-ITD (20 nM) was incubated with yeast PCNA (100 nM) and ^{32}P-labeled DNA substrate (100 nM) in reaction buffer (20 mM Tris-HCl, pH 7.8, 1 mM DTT, 100 μg/mL BSA, 8 mM $MgOAc_2$, and 1 mM spermidine) with or without each of the four deoxyribonucleotides (100 μM each) and ATP (1 mM), at 30℃ for 2.5, 5, 10, 20, or 40 min. The reactions were stopped by addition of 2 × loading buffer (25 mM EDTA, 0.2% bromophenol blue, and 0.2% xylene cyanol) followed by boiling for 10 min. The reaction was resolved using 15% denaturing PAGE and visualized using radioautography.

To reconstitute the sequential reactions of 3' flap cleavage, gap filling, and DNA ligation, a 3' flap DNA substrate (100 nM) was incubated with Polδ (20 nM) in reaction buffer (20 mM Tris-HCl, pH 7.8, 1 mM DTT, 100 μg/mL BSA, 8 mM $MgOAc_2$, and 1 mM spermidine) with or without each of the four deoxyribonucleotides (100 μM each) and ATP (1 mM), at 30℃ for 10 min. Purified recombinant yeast DNA Lig I (75 nM) was added to the reaction, and DNA

ligation was allowed to proceed during a 10 min incubation (30°C) or the reaction was immediately stopped by addition of 2 × loading buffer to serve as an unligated control. Ligation reactions were also stopped by addition of 2 × loading buffer and all samples were boiled for 10 min. Reactions were then resolved using 15% denaturing PAGE and visualized using radioautography. The 5' ^{32}P-labeled 3' flap DNA substrates S1-S8 were prepared using the synthetic oligonucleotides listed in Tables S5 and S6.

Western blot analysis of chromatin-associated Dun1 and Flag-tagged Pol3

Chromatin-associated proteins were isolated from yeast cells as previously described (*39*). Briefly, harvested yeast cells were suspended in a buffer containing 0.1 M K-EDTA, pH 8.0, 10 mM DTT and incubated at 30°C for 10 min. After centrifugation, the cell pellet was resuspended in YPD medium containing 1 M sorbitol, 10 U/mL Zymolyase (AMSBIO, 120491-1) and incubated at 37°C for 1 h. After centrifugation, the pellet was resuspended in extraction buffer (50 mM HEPES/KOH pH7.5, 150 mM KGlu, 2.5 mM $MgOAc_2$, 0.1 mM $ZnOAc_2$, 1 mM DTT, 1 mM PMSF, protein inhibitor, phosphatase inhibitor, 0.25% Triton X-100) and incubated on ice for 10 min. The whole cell extract was then loaded onto extraction buffer containing 30% sucrose. After centrifugation (15,000 × *g*, 10 min) at 4ºC, the pellet (chromatin fraction) was dissolved in SDS-PAGE loading buffer and resolved using 8% SDS-PAGE. Immunoblot was conducted to analyze the chromatin-associated Dun1 using a polyclonal anti-yeast Dun1 antibody (from Wolf-Dietrich Heyer lab). Histone H2B, which was detected by immunoblot using a polyclonal anti-yeast Histone H2B (Ab18829, Abcam), was used as a chromatin marker and loading control.

To detect Flag-tagged WT or ITD Pol3, the whole cell extract was prepared and dissolved SDS-PAGE loading buffer and resolved using 8% SDS-PAGE. Immunoblot was conducted to analyze the Flag-tagged WT or ITD Pol3 using the monoclonal anti-Flag tag antibody. Ponceau S staining of total proteins was used as a loading control.

3' flap labeling of genomic DNA

3' flaps in yeast genomic DNA were labeled using an approach that was modified from protocols for labeling single-strand DNA (ssDNA) breaks in the genome (*40, 41*). High molecular weight genomic DNA from WT or *rad27*Δ cells grown at 30°C with or without exposure to 37°C (4 h) was isolated following the protocol for isolating yeast genomic DNA for detection of ssDNA breaks by sequencing (GLOE-Seq) (*41*). Following the protocol for nick sequencing (Nick-seq) (*40*), genomic DNA was fragmented by incubation with the restriction enzymes Hind III, Xba I, and Xho I, which generates 4 nt 5' overhangs at the DNA ends. The 3' OH at DNA nicks/gaps or at DNA ends was blocked with dideoxyribonucleotides by incubation with the 3' exonuclease-deficient Klenow fragment (37ºC, 1 h). The free 3' OH at the 3' flap, which was not blocked by the 3' exonuclease-deficient Klenow fragment, was labeled with ^{32}P-deoxyribonucleotides by terminal DNA transferase (37ºC, 1 h). The ^{32}P-labeled genomic DNA was denatured using 2 × denaturing PAGE loading buffer, resolved using 5% denaturing PAGE, and visualized using

radioautography. The total input DNA prior to ^{32}P labeling was resolved using gel electrophoresis (1% agarose) and visualized using SYBR green staining.

Gene expression profiling by RNA-seq and enrichment analysis

Total RNA from WT or *rad27*Δ cells grown at 30℃ with or without exposure to 37℃ (4 h) was isolated using the RNeasy Mini kit (Qiagen). Two independent biological replicates were used for each group. Sequencing libraries were prepared using the TruSeq RNA Sample Prep Kit V2 (Illumina) according to the manufacturer's protocol. The cDNA libraries were prepared for sequencing using the cBot cluster generation system with the HiSeq SR Cluster Kit V4 (Illumina). Sequencing was performed in single-read mode for 51 cycles of read 1 and 7 cycles of index read using the HiSeq 2500 platform with the HiSeq SBS Kit V4 (Illumina). The real-time analysis 2.2.38 software package was used to process the image analysis and base calling. RNA-seq reads were trimmed to remove sequencing adapters by using Trimmomatic and to remove polyA tails by using FASTP. The processed reads were mapped back to the *S. cerevisiae* S288C genome assembly R64 (SacCer3) using STAR software v. 020201. HTSeq v.0.6.0 was applied to generate the count matrix of refSeq genes with default parameters. Differential expression analysis was conducted after normalizing the raw counts using the TMM (Trimmed Mean of M-values) normalization method in the "edgeR" package (*42*). Genes with a false discovery rate less than 0.05, a p value less than 0.05, and a fold-change greater than 1.5 or less than 0.67 were considered significantly up- or down-regulated, respectively. The sets of genes that were categorized as Dun1-, Mec1-, Rad53-, or Tel1-dependent were retrieved from a previous study (*43*). The hypergeometric test (*44*) was used to determine if the set of up-regulated or down-regulated genes in *rad27*Δ or/and due to heat stress were Dun1-, Mec1-, Rad53-, or Tel1-dependent.

WGS and WES analysis

Total DNA from WT and *rad27*Δ yeast cells with or without knock-in of a *pol3* mutation and grown at 30℃ or 37℃ was isolated using the YeaStar Genomic DNA kit (ZYMO Research, D2002). For sequencing library preparation, 40 ng of yeast genomic DNA from each sample was fragmented using a Covaris LE220-plus with a peak size setting of 250 bp. The libraries were prepared using the Kapa DNA HyperPrep Kit (Kapa, Cat KK 8700) according to the manufacturer's protocol with 4-cycles of PCR. Libraries were sequenced on an Illumina HiSeq2500 using a paired end mode of 2 × 101 cycles. Two independent biological replicates were used for each group. Reads were filtered using Cutadapt v1.18 to remove low-quality reads and sequencing adapters and were aligned to the SacCer3 reference genome using NovoAlign v3.02.07. Only reads that aligned to unique genome locations were kept for variant calling. Samtools v1.10 and VarScan v.2.3.9 (*45*) were used to identify somatic single nucleotide variants and small indels. Structural variants such as classic or alternative duplications were detected by Pindel (*46*) using default parameters. To calculate the mutation frequency, germline mutations that were detected in both WT and *rad27*Δ or in both *rad27*Δ and *rad27*Δ *pol3* knock-in double mutants were filtered out, and the counts of each type of mutation were divided by the number of base pairs in the yeast genome.

Duplications in normal lung and lung tumors from WT or A159V/WT mice and in human B cell acute lymphoblastic leukemia (ALL) were analyzed in WES data using the Pindel program (*46*). WES data from three human B cell ALL patients (#121, #798, and #985) were randomly selected from a published WES dataset of paired tumor vs. normal tissues (peripheral blood samples collected after complete remission) (*47*). WES was conducted on genomic DNA isolated from normal lung and lung tumors from WT or A159V/WT mice as previously described (*48*). Duplications were scored if at least three supporting tracks were detected. The intervening spacer DNA sequences detected in the mouse or human specimens were mapped to the mouse or human genome, respectively, using the BLAT function of the UCSC genome browser (*49*). The frequencies of the duplications were estimated by dividing the number of duplications by the size of the mouse exome (~30 million base pairs) or human exome (~30 million base pairs).

Statistical analysis

Two-tailed student's t-test was used to determine significance in differences in mutation rate assays and the hypergeometric test was used to determine the significance in the enrichment of a signaling pathway. Fisher exact test was used to determine the significance of cancer incidence between the treated and untreated groups.

Supplementary Text

S1. Mapping the Pol3 mutations detected in the revertants to the functional domains of Pol3

An in-frame internal tandem duplication ([ITD]; 458–477) and four point mutations (R470G, R475I, A484V, and H495Q) occurred within the Pol3 nuclease domain near the Exo II (Nx3F/YD), Exo III (Yx3D), and Pol IV motifs (Fig. 1B). We also identified an in-frame ITD (591–598) within the Pol II motif, an S847Y mutation within the Pol V motif, and a P965T mutation in motif 3 of the C-terminal domain (CT3) (Fig. 1B).

S2. Genetic crosses of the *rad27*Δ *pol3* ITD strain with the *exo1*Δ or the *dna2-1* strain.

*rad27*Δ cells display synthetic lethality with *exo1* or *dna2* deficiency (*26*, *27*). To determine if *pol3* ITD could suppress such lethality, we conducted genetic crosses to create spores carrying *rad27*Δ *pol3* ITD *exo1*Δ or *rad27*Δ *pol3* ITD *dna2-1* triple-mutant alleles. In the cross between *rad27*Δ::*LEU2 pol3* ITD::*HIS3* and *exo1*Δ::*URA3* strains, 2788 colonies grew on YPD plates, but only 18 colonies grew on SC-Leu-His-Ura selection plates (Table S2). The viable spore ratio (0.006) of *rad27*Δ *pol3* ITD *exo1*Δ was markedly less than the expected spore ratio (0.125), indicating the triple-mutant was lethal. Similarly, in the control cross between *rad27*Δ::*LEU2* and *exo1*Δ::*URA3* strains, 2865 colonies grew on YPD plates, but only 26 colonies grew on SC-Leu-Ura selection plates (Table S2). The viable spore ratio (0.009) of *rad27*Δ *exo1*Δ was markedly less than the expected spore ratio (0.25), indicating the double-mutant was lethal. This

is consistent with a previous study showing that *rad27*Δ *exo1*Δ cells are inviable (*27*). In contrast, in the cross between *pol3* ITD::*HIS3* and *exo1*Δ::*URA3* strains, 2288 and 610 colonies grew in the YPD and SC-His-Ura plates, respectively (Table S2). The viable spore ratio (0.27) of *pol3* ITD *exo1*Δ was close to the expected *pol3* ITD *exo1*Δ spore ratio (0.25), indicating that *pol3* ITD in combination with *exo1*Δ results in viable spores.

The *dna2-1* allele (P504S) has no selection marker. Therefore, we used PCR-based DNA sequencing to genotype the *DNA2* mutation in the yeast cells. In the cross between *rad27*Δ::*LEU2 pol3* ITD::*HIS3* and *dna2-1* strains, *rad27*Δ *pol3* ITD cells grown on the SC-Leu-His plate were genotyped. Of 60 independent *rad27*Δ *pol3* ITD colonies sequenced, no *dna2-1* allele was detected (Table S3). In the control cross between *rad27*Δ::*LEU2* and *dna2-1* strains, no *dna2-1* allele was detected in 40 independent *rad27*Δ colonies (Table S3). This is consistent with a previous study showing that *rad27*Δ *dna2-1* cells are inviable (*26*), However, 18 out of 38 independent colonies carried the *dna2-1* allele from the cross between *pol3* ITD::*HIS3* and *dna2-1* strains (Table S3). The viable spore ratio (0.47) agreed with the expected *pol3* ITD *dna2-1* ratio (0.5), indicating that *pol3* ITD in combination with *dna2-1* results in viable spores.

S3. Three types of hairpin-forming alternative duplications in *rad27*Δ cells grown at 37ºC.

We observed three types of alternative duplications based on hairpin structure-forming sequence features. In type 1 alternative duplications, the 5’ DNA sequence of the downstream duplication unit could form a 5’ fold-back structure (Fig. 2D, fig. S4A), while the 3’ end of the upstream duplication unit was complementary to nearby downstream DNA sequences (orange highlighted segment, fig. S4A), allowing potential invasion and extension into the downstream DNA duplex. The DNA sequence of the spacer (green segment) corresponded to the predicted extended DNA sequence of the 3’ end of the upstream duplication unit (Fig. 2D, fig. S4A, S4B). In type 2 alternative duplications, the 3’ sequence of the duplication unit could form a 3’ fold-back structure and the predicted extension of this 3’ fold-back corresponded to the spacer (green segment, fig. S4A, S4C). The 5’ sequence of the downstream duplication unit was complementary to the nearby upstream DNA sequences (orange highlighted segment, fig. S4A), allowing strand exchange and producing a ligatable nick (Fig. 2D, fig. S4A, fig. S4C). Similar to the type 2 alternative duplications, type 3 duplications also had a 3’ fold-back structure-forming DNA sequence and the spacer corresponded to the predicted extended DNA sequence of the 3’ fold-back (Fig. 2D, fig. S4A, S4D). However, the 3’ end of the spacer was complementary to the DNA sequence on the template strand near the 5’ end of the upstream duplication unit (orange highlighted segment, fig. S4A). This sequence feature allowed strand exchange to generate a ligatable DNA nick (Fig. 2D, fig. S4D).

S4. Reconstitution of 3’ flap-based OFM

To define 3’ flap-based OFM and the formation of alternative duplications, we reconstituted the sequential reactions of 3’ flap cleavage, DNA synthesis, and ligation of oligo-based DNA substrates with 3’ flaps of 10 or 20 nt to represent 3’ flaps that were converted from short 5’ flaps (S2 and S3, fig. S5B). We found that Polδ could effectively cleave a 3’ flap of 10 or 20 nt

and stop at the junction of the 3’ flap and DNA duplex in the presence of deoxyribonucleotides, generating ligatable DNA nicks for DNA Lig I (Fig. 2H and fig. S5). The ssDNA binding protein RPA did not block Polδ-mediated 3’ flap cleavage or subsequent nick ligation (Fig. 2H). To determine if formation of a hairpin structure from the 3’ flap could lead to alternative duplications, we reconstituted 3’ flap-based OFM using the DNA substrates S4 and S5, which resemble type I or type II alternative duplication, respectively (Fig. 2I). In the absence of deoxyribonucleotides, Polδ cleaved the 3’ flap in S4, producing a gapped DNA duplex (Fig. 2I). However, in the presence of deoxyribonucleotides, an extended unligated product of ~85 nt was produced, which was ligated with the fold-back 5’ flap by Lig I to form a ligated extended product (~160 nt, Fig. 2I). We found that the 3’ flap fold-back structure in S5 was resistant to cleavage by the 3’ nuclease activity of Polδ even in the absence of deoxyribonucleotides. Addition of deoxyribonucleotides to the reaction led to extension of the 3’ flap fold-back into a ~95 nt product, which was ligated into a product of ~160 nt (Fig. 2I). RPA slightly enhanced formation of the ligated extended products (Fig. 2I). These data suggest that 3’ flap-based OFM may result in alternative duplications, including mutations with features similar to *pol3* 458–477 ITD. However, we also found that when extension of the annealed 3’ flap could not generate ligatable nicks, only unligated extended products were produced (fig. S6A-6D), leading to failure of 3’ flap-based OFM. The reconstitution assays showed that the 3’ nuclease activities of Polδ and Lig I are sufficient to complete 3’ flap processing for OFM.

S5. 3’ flap cleavage patterns by recombinant Polδ and NE

The 3’ flap cleavage pattern produced using purified recombinant Polδ for a simple 3’ flap was similar to that produced by NE from WT cells (fig. S7A). Both could remove a 3’ flap at the ssDNA-dsDNA junction. However, purified recombinant Polδ but not NE further effectively cleaved the intermediate DNA nick, producing DNA gaps. Purified Polδ failed to cleave hairpin-forming 3’ flaps, but NE from WT cells effectively cleaved hairpin-forming 3’ flaps around the dsDNA-ssDNA junction (fig. S7B). However, NE from *rad27*Δ cells, especially those grown at 37°C, showed greatly reduced activity in processing simple or hairpin-forming 3’ flaps (fig. S7A, S7B).

S6. Revertant frequency in *rad27*Δ and *rad27*Δ *dun1*Δ cells

To determine the impact of Dun1 signaling on the generation of *rad27Δ* revertants, we measured the revertant frequency in *rad27*Δ and *rad27*Δ *dun1*Δ cells following increasing periods of exposure to the restrictive temperature (37°C). Prior to incubation at 37°C, both *rad27*Δ and *rad27*Δ *dun1*Δ cells had similarly low revertant frequencies (~0.02%, Fig. 4E). Incubation of *rad27*Δ cells at 37°C for 2–8 h led to a more than 15-fold increase in the revertant frequency to ~0.3%. In contrast, incubation of *rad27*Δ *dun1*Δ cells at 37°C for 2–8 h had little effect on the revertant frequency (Fig. 4E). Both *rad27*Δ and *rad27*Δ *dun1*Δ cells exposed to heat stress for 24 h showed increased revertant frequencies of ~1.0% or ~0.2%, respectively (Fig. 4E). This marked increase in revertant frequency at 24 h was likely mainly due to amplification of selected revertants rather than the generation of new revertants.

S7. Impact of Chk1 inhibition on cancer development in FEN1 mutant mice

Functional deficiency due to FEN1 (the mammalian homolog of Rad27) mutations promotes DNA mutations and chromosome arrangements, leading to a high frequency of cancer in mice (*50*). This suggests that FEN1 mutant tumor-initiating cells can overcome OFM defects and replication stress. We previously observed that the FEN1 F343A/F344A (FFAA) mutation, which disrupts the FEN1/PCNA interaction and recruitment of FEN1 to replication forks, resulted in unligated Okazaki fragments and activation of the Chk1 signaling pathway (*32*). Heterozygous FFAA mutant mice develop lung adenoma and adenocarcinoma at high frequencies (*32*). To determine if cancer development in FEN1 FFAA mutant mice depends on activation of the Dun1 functional analogue, Chk1, we treated WT and FFAA mice with the Chk1 inhibitor SB218078 (*51*). This treatment significantly inhibited spontaneous lung cancer development in WT/FFAA mice but not in WT mice (Fig. S15). These results suggest that suppression of stress-induced DNA damage response signaling is an effective approach for chemoprevention and may provide a new way to inhibit drug resistance.

S8. Impact of deoxyribonucleotides on 3' flap processing and mutations

Restrictive temperature stress activates Dun1, which up-regulates expression of *HUG1*, *RNR2*, *RNR3*, and *RNR4* for *de novo* production of deoxyribonucleotides. We determined that impact of deoxyribonucleotides on processing of 3' flaps by Polδ *in vitro*. In the absence of deoxyribonucleotides, Polδ effectively cleaved the 3' flap as well as intermediate DNA nicks (fig. S5). Deoxyribonucleotides did not affect Polδ 3' flap cleavage activity but did inhibit the 3' exonuclease activity of Polδ to cleave the intermediate DNA nick, and switched the function of Polδ to gap-filling DNA synthesis (fig. S5). Increasing the deoxyribonucleotide concentration did not affect 3' flap processing but promoted 3' flap extension and increased levels of unligated and ligated extended products in reconstitution assays (fig. S16A-C). In addition, it has been suggested that the 3' exonuclease activity of Polδ could degrade the upstream Okazaki fragment from the 3' end to create a gap (*16, 23*). The 5' flap could re-anneal into the gap and be resolved if this process occurred during OFM. However, we discovered that in the presence of deoxyribonucleotides, creation of such a gap by the 3' exonuclease activity of Polδ on a nicked DNA substrate with no 3' flap (S1) or with a 1 nt 3' flap (S8), representing 3' end fraying (*23*), was greatly inhibited (fig. S17). Thus, an increase in deoxyribonucleotide production due to Dun1 activation suppresses gap formation by the 3' exonuclease activity of Polδ and pushes the process toward 3' flap-based OFM and generation of *pol3* 458–477 ITD, which leads to revertant development.

We further tested whether up-regulation of deoxyribonucleotides promotes DNA mutations *in vivo*. We found that *SML1* deletion, which results in increased dNTP pools but does not affect other Dun1-mediated cellular processes (*19*), did not increase mutation rate in either WT or *rad27*Δ cells (fig. S18), suggesting that up-regulation of dNTP levels alone is not sufficient to promote mutations.

S9. 3' flap OFM-related alternative duplications in mouse and human cancers.

We sought to determine the human cancer relevance of 3' flap-based OFM and the related alternative duplications. We noticed that the alternative duplications observed in *rad27*Δ cells grown at 37°C consisted of a duplication unit (less than 100 bp in length) and a short intervening spacer sequence that could be mapped to the nearby DNA sequence (usually no farther than 100 bp). Such alternative duplications may be produced through the 3' flap-based OFM pathway, therefore we defined them as 3' flap OFM-related alternative duplications. To evaluate the status of these duplications in human cancers, we re-analyzed a published WES dataset of paired tumor vs. normal tissue (peripheral blood samples collected during complete remission) (*47*). WES data from three randomly selected B cell ALL patients were analyzed using the Pindel program to define the duplications in these cancer specimens. We found that the frequencies of germline alternative duplications in the peripheral blood of patients #121 and #985 were relatively low, but the frequencies of somatic alternative duplications in the cancer samples were remarkably higher than the corresponding germline duplications (fig. S19A). Frequencies of both the germline and somatic alternative duplications in patient #798 were relatively low (fig. S19A). The lengths of spacers in the alternative duplications in the three ALL specimens ranged from 1 nt to 70 nt (fig. S19B). This was similar to the spacer lengths we observed for stress temperature-induced alternative duplications in *rad27*Δ yeast (Fig. 2B). To further define the origin of these spacer sequences and evaluate the frequency of 3' flap OFM-related alternative duplications, we mapped the spacer DNA sequences across the human genome. We detected 0.6, 0.2, and 0.9 3' flap OFM-related alternative duplications per million bases in patients #121, #798, and #985 respectively (fig. S19C).

FEN1 mutations have been detected in human cancers and functional deficiency in FEN1 has been linked to cancer initiation and progression and to development of resistance to cancer therapies (*20, 33, 50*). Therefore, FEN1 mutations in human cancers may lead to 3' flap-based OFM, and thus play crucial roles in cancer cell evolution, tumor growth, and resistance to cancer therapy. To determine if FEN1 mutations had a positive correlation with 3' flap OFM-related alternative duplications, we conducted WES on normal lung and lung tumor tissues from WT and FEN1 A159V/WT mice, which are an appropriate model for human lung cancer patients carrying the A159V FEN1 mutation (*20,33*). We observed that normal lung tissues from the A159V/WT mouse but not normal lung tissues from the WT mouse had somatic 3' flap OFM-related alternative duplications (fig. S19D). We also found that both A159V/WT and WT lung tumor tissues had considerably more 3' flap OFM-related alternative duplications than the corresponding normal lung tissues, but that the alternative duplication frequency in the A159V/WT lung tumors was considerably higher than in the WT tumors (fig. S19D). These findings suggest that FEN1 deficiency promotes 3' flap OFM-related alternative duplications, which have a positive correlation with cancer development, even in the WT FEN1 genetic background.

Fig. S1.

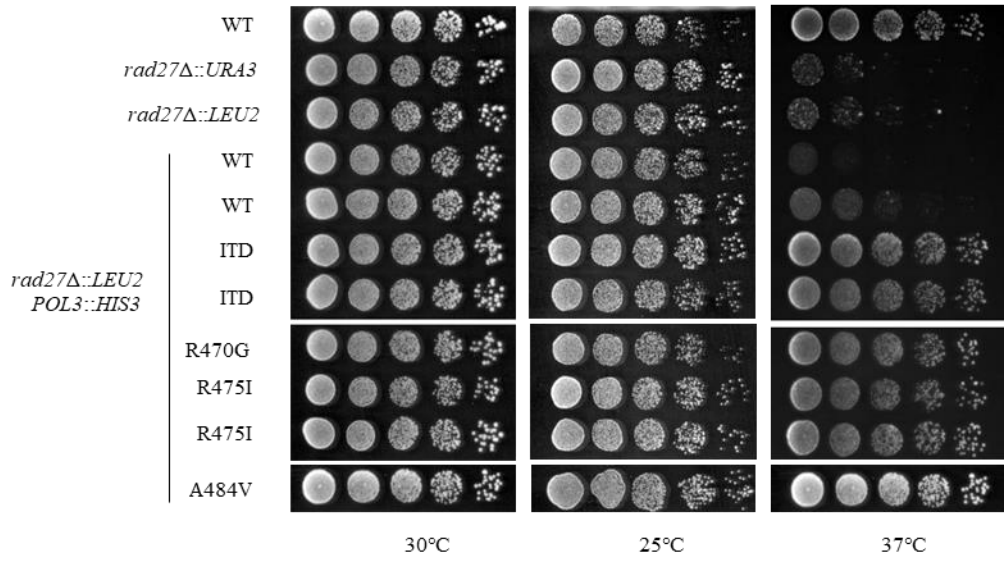

Fig. S1. Knock-in of *pol3* mutations in *rad27*Δ cells reverses conditional lethality at 37°C. Viability of WT, *rad27*Δ, and *rad27*Δ cells carrying the WT or the *pol3* mutant allele (ITD, R470G, R475I, or A484V) was analyzed using spot assays. Yeast cells of the indicated genetic backgrounds were serially diluted, spotted onto YPD plates, and incubated at 30°C, 25°C, or 37°C for 48 h. *rad27*Δ::*URA3* or *rad27*Δ::*LEU2* represent the *rad27*Δ allele with a linked *URA3* or *LEU2* selection marker gene, respectively.

Fig. S2.

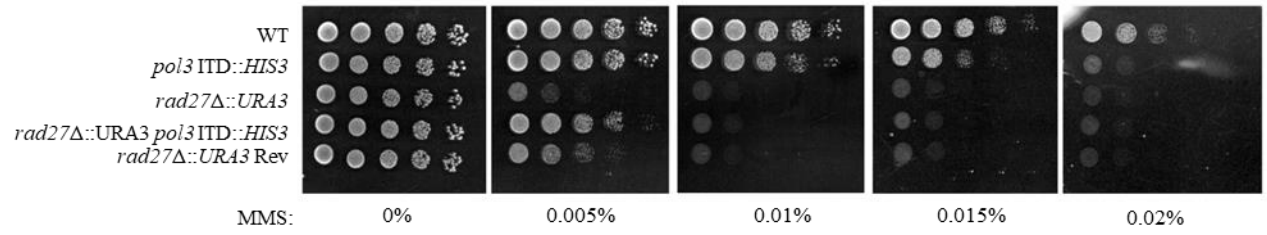

Fig. S2. *pol3* ITD-bearing *rad27*Δ revertant mutations or *pol3* ITD knock-in of *rad27*Δ cells partially reverse MMS-induced lethality. Viability of WT, *pol3* ITD knock-in, *rad27*Δ, *rad27*Δ with the *pol3* ITD knock-in mutation, and a *rad27*Δ revertant carrying a *pol3* ITD mutation was analyzed using spot assays. Yeast cells of the indicated genetic backgrounds were serially diluted and spotted on YPD plates containing the indicated level of MMS. The plates were incubated at 30℃ for 48 h.

Fig. S3.

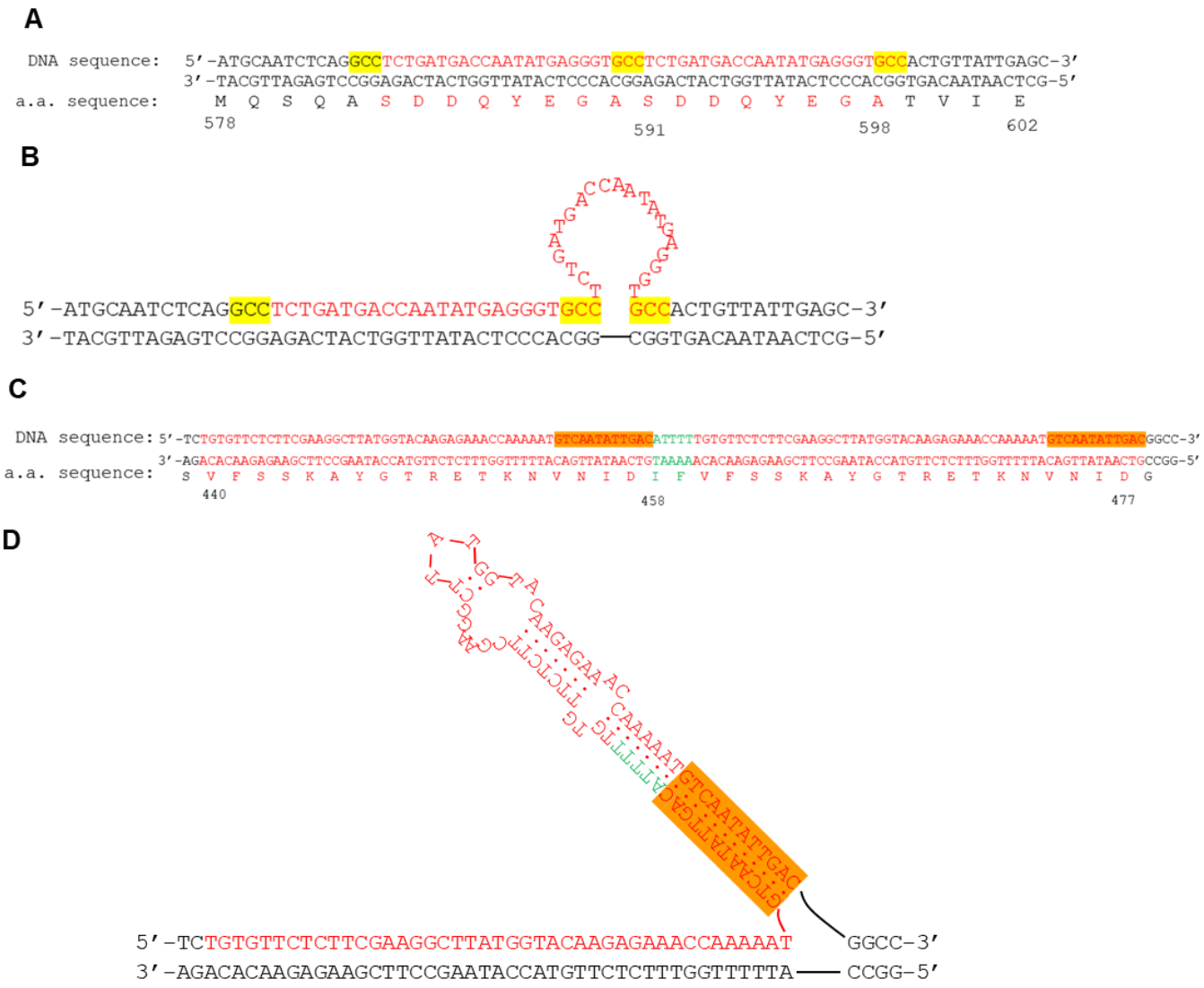

Fig. S3. *pol3* ITD mutations that occurred in *rad27*Δ DNA sequences. (A) Red, DNA and amino acid (a.a.) sequences of the classic duplication: *pol3* 591-598 ITD; yellow highlights, three repeat DNA sequence for duplication formation via 5' annealing as illustrated in panel B. **(B)** The predicted loop structure that results in the *pol3* 591-598 ITD. The repeat sequence (yellow highlight) at the 5' end of the downstream duplication unit anneals to its complementary sequence of the repeat sequence (yellow highlight) at the 3' end of the upstream duplication unit, producing a nick. Ligation of the DNA nick produces the classic duplication, *pol3* 591-598 ITD. **(C)** Red, DNA and amino acid (a.a.) sequences comprising the duplication unit of the alternative duplication, the *pol3* 458-477 ITD; green, DNA and a.a. sequences comprising the spacer between the duplication units; orange highlights, DNA sequences that are complementary elements that can anneal for extension and formation of repairable nicks/gaps as shown in panel D. **(D)** The predicted secondary structure that results in the *pol3* 458-477 ITD. The 3' end of the upstream duplication unit (orange highlights) anneals to its complementary sequence (orange highlights) at the downstream duplication unit. Extension of the annealed 3' end produces the spacer DNA sequence (green). Secondary structure predication was carried out using the RNAFold program.

Fig. S4.

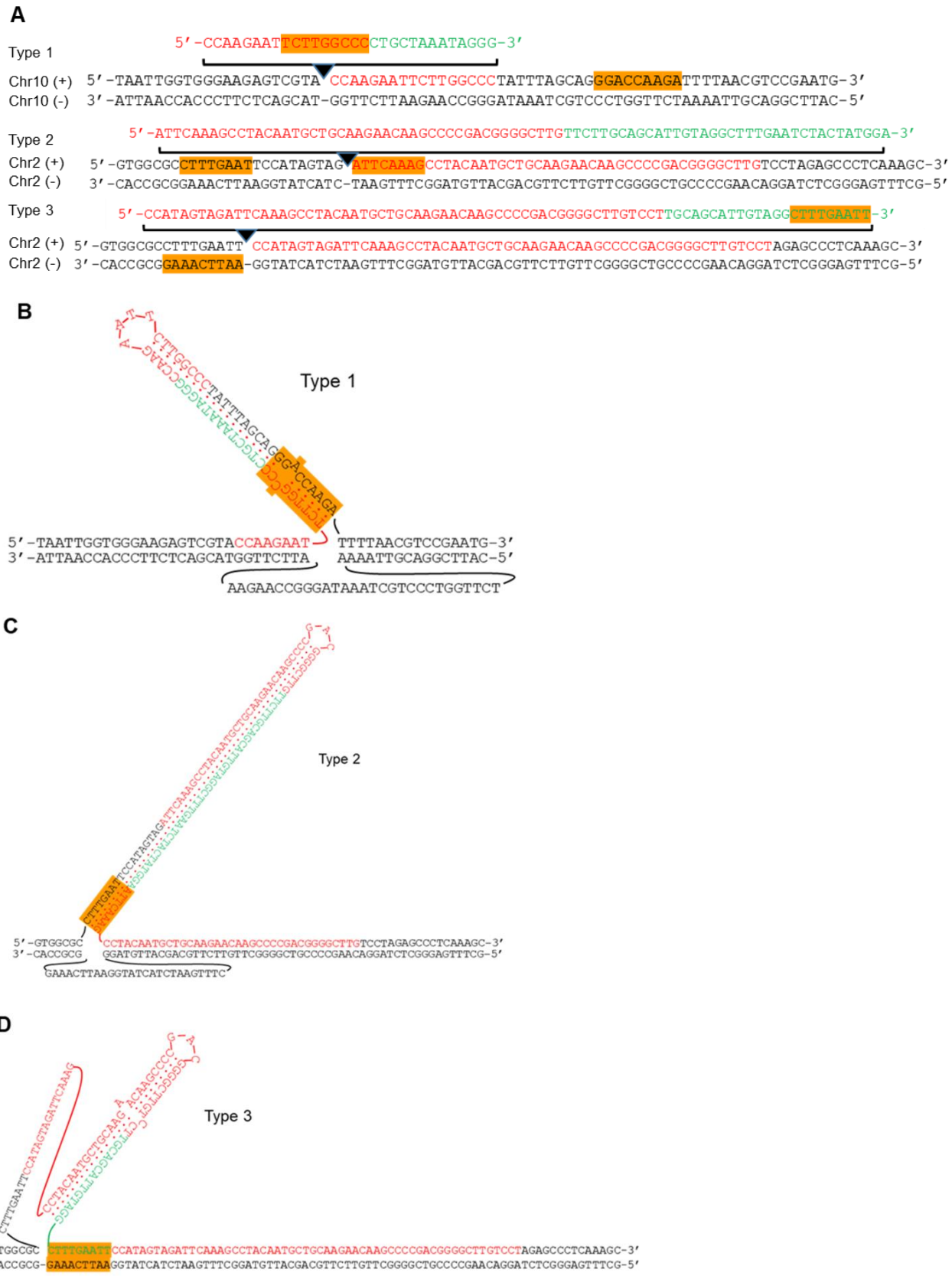
A
Type 1
5′-CCAAGAATTCTTGGCCCCTGCTAAATAGGG-3′
Chr10 (+) 5′-TAATTGGTGGGAAGAGTCGTACCAAGAATTCTTGGCCCTATTTAGCAGGGACCAAGATTTTAACGTCCGAATG-3′
Chr10 (-) 3′-ATTAACCACCCTTCTCAGCAT-GGTTCTTAAGAACCGGGATAAATCGTCCCTGGTTCTAAAATTGCAGGCTTAC-5′
Type 2
5′-ATTCAAAGCCTACAATGCTGCAAGAACAAGCCCCGACGGGGCTTGTTCTTGCAGCATTGTAGGCTTTGAATCTACTATGGA-3′
Chr2 (+) 5′-GTGGCGCCTTTGAATTCCATAGTAGATTCAAAGCCTACAATGCTGCAAGAACAAGCCCCGACGGGGCTTGTCCTAGAGCCCTCAAAGC-3′
Chr2 (-) 3′-CACCGCGGAAACTTAAGGTATCATC-TAAGTTTCGGATGTTACGACGTTCTTGTTCGGGGCTGCCCCGAACAGGATCTCGGGAGTTTCG-5′
Type 3
5′-CCATAGTAGATTCAAAGCCTACAATGCTGCAAGAACAAGCCCCGACGGGGCTTGTCCTTGCAGCATTGTAGGCTTTGAATT-3′
Chr2 (+) 5′-GTGGCGCCTTTGAATTCCATAGTAGATTCAAAGCCTACAATGCTGCAAGAACAAGCCCCGACGGGGCTTGTCCTAGAGCCCTCAAAGC-3′
Chr2 (-) 3′-CACCGCGGAAACTTAA-GGTATCATCTAAGTTTCGGATGTTACGACGTTCTTGTTCGGGGCTGCCCCGAACAGGATCTCGGGAGTTTCG-5′
B
Type 1
5′-TAATTGGTGGGAAGAGTCGTACCAAGAATTTTTAACGTCCGAATG-3′
3′-ATTAACCACCCTTCTCAGCATGGTTCTTAAAAATTGCAGGCTTAC-5′
AAGAACCGGGATAAATCGTCCCTGGTTCT
C
Type 2
5′-GTGGCGCCCTACAATGCTGCAAGAACAAGCCCCGACGGGGCTTGTCCTAGAGCCCTCAAAGC-3′
3′-CACCGCGGGATGTTACGACGTTCTTGTTCGGGGCTGCCCCGAACAGGATCTCGGGAGTTTCG-5′
GAAACTTAAGGTATCATCTAAGTTTC
D
Type 3
5′-GTGGCGCCTTTGAATTCCATAGTAGATTCAAAGCCTACAATGCTGCAAGAACAAGCCCCGACGGGGCTTGTCCTAGAGCCCTCAAAGC-3′
3′-CACCGCG-GAAACTTAAGGTATCATCTAAGTTTCGGATGTTACGACGTTCTTGTTCGGGGCTGCCCCGAACAGGATCTCGGGAGTTTCG-5′

Fig. S4. Representative DNA sequences (A) and predicted hairpin structure (B-D) of the three types of alterative duplications detected in *rad27*Δ cells (37°C, 4 h). Red, DNA sequences comprising the duplication unit; green, DNA sequences comprising the spacers between the duplication units; orange highlights, DNA sequences that are complementary elements (with or without a mismatch) that can anneal for extension and formation of repairable nicks/gaps. Predicted hairpin structures of three representative alternative duplications. Panels B, C, and D show the predicted Type 1, Type 2, and Type 3 alternative duplications, respectively. Secondary structure predication was carried out using the RNAFold program.

Fig. S5.

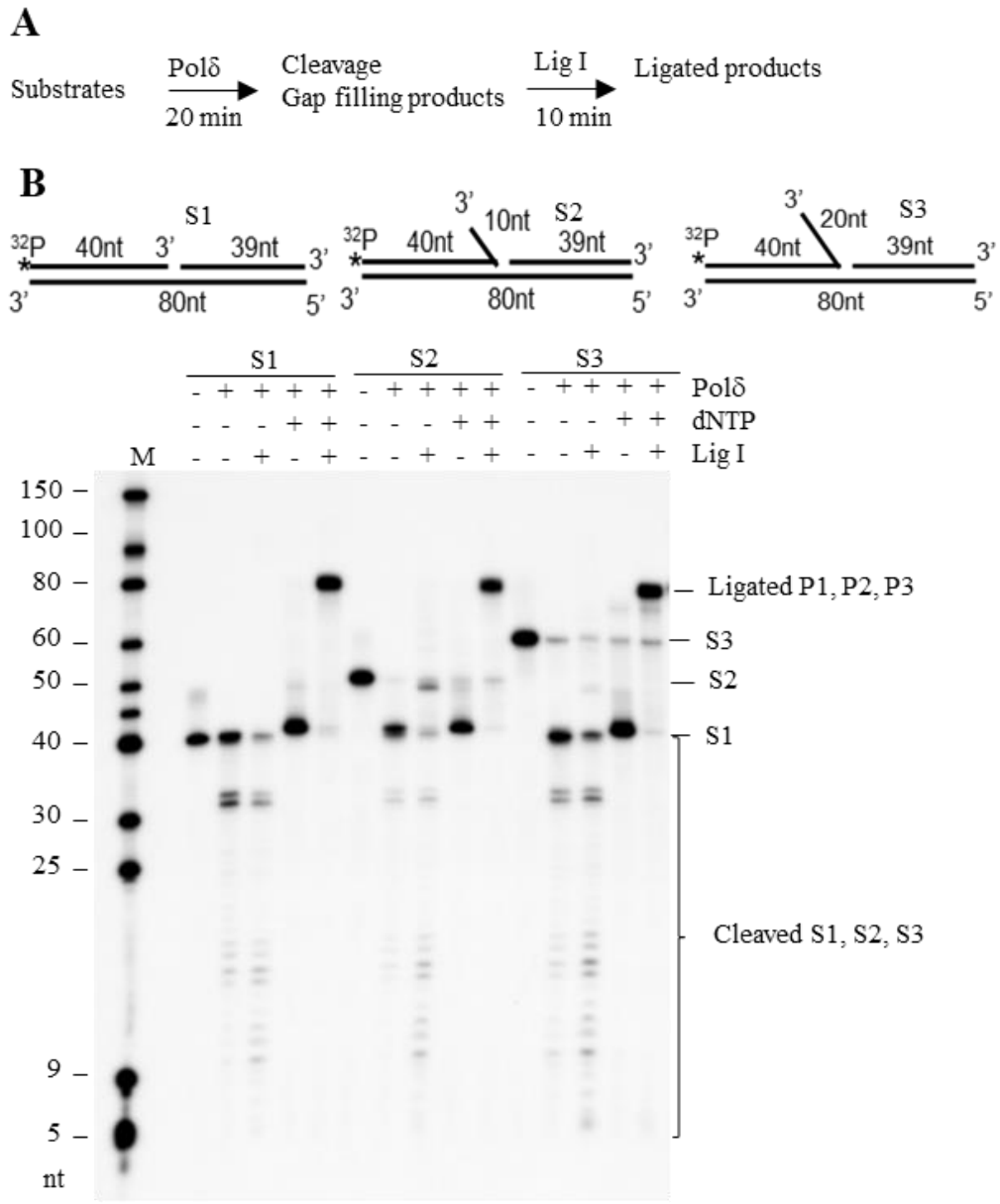

Fig. S5. Reconstitution assays using ^{32}P-labeled 3' flap substrate. (A) Schematic of sequential reconstitution of Polδ-mediated OFM involving 3' flap cleavage, gap filling, and DNA ligation. **(B)** Reconstitution assays (30°C). Top panels: Diagrams of DNA substrates with a 1 nt gap and a 3' flap of 0 (S1), 10 (S2), or 20 nt (S3) that were used for the assays. Bottom panel: Representative PAGE image of the assay. DNA substrates (S1, S2, S3), cleavage products (Cleaved S1, S2, S3), and ligated products (Ligated P1, P2, P3) are indicated.

Fig. S6.

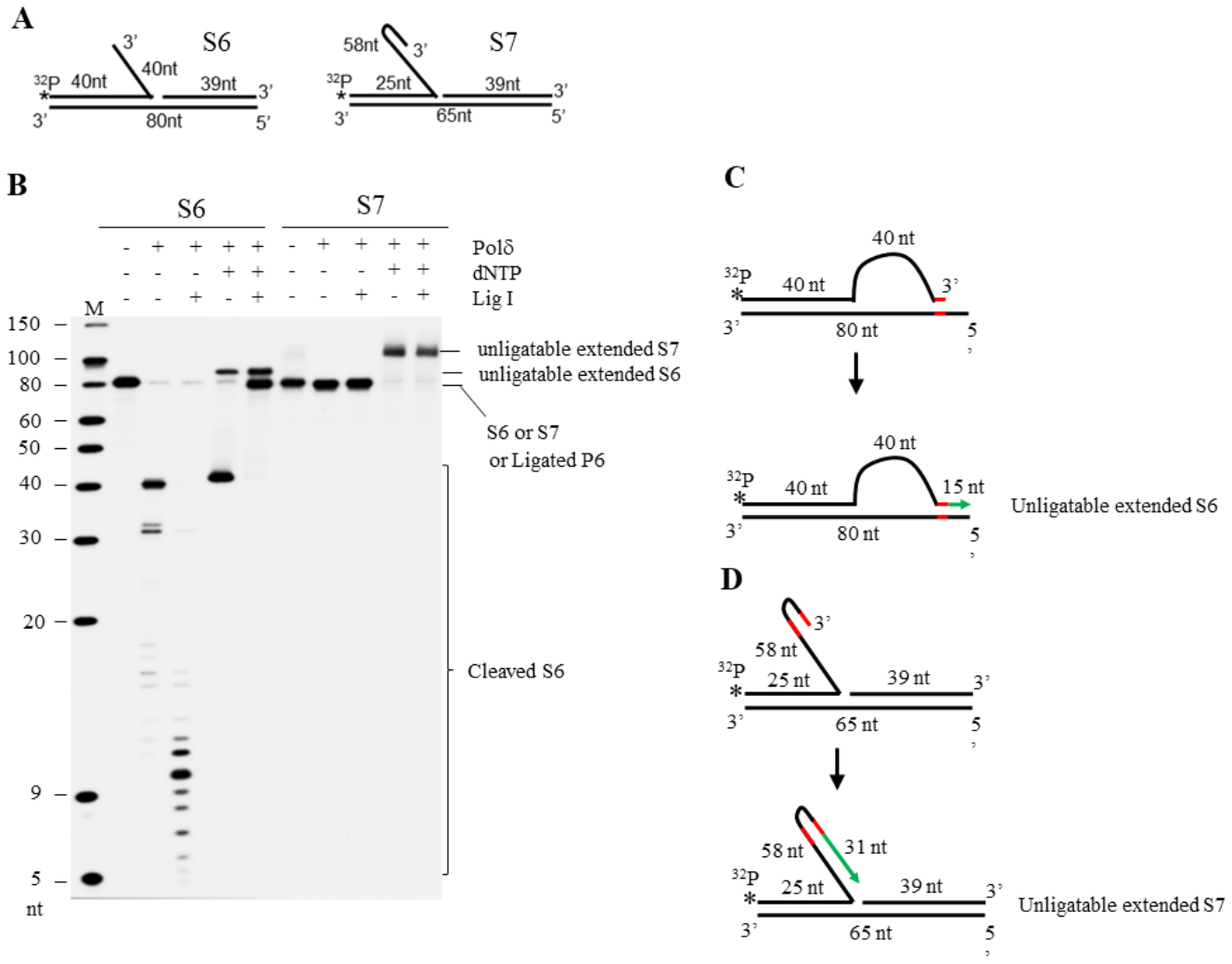

Fig. S6. Reconstituted 3' flap-based OFM on DNA substrates with long 3' flaps. (A) Diagrams of DNA substrates with a 1 nt gap and a 3' flap of 40 nt (S6) or a fold-back forming 3' flap (S7) that were used for the assays shown in panel B. **(B)** Representative reconstitution assays (30°C) for 3' flap-based OFM on DNA substrates S6 and S7. DNA substrate, cleavage products, unligated, and extended products (unligatable extended S6 or S7) are indicated. Substrates and products were analyzed using 15% denaturing PAGE. **(C)** Schematic elucidating formation of unligatable extended products in reactions using the 3' flap substrate S6. Mis-alignment of the 3' flap with the template via a 4 nt microhomology sequence (red), which is 15 nt from the 5' end of the template, prevented its degradation by the 3' exonuclease activity of Polδ. Extension of this structure (green) resulted in a 95 nt unligatable extended product (unligatable extended S6). **(D)** Formation of fold-back secondary structure in a 3' flap via the homology sequence (red) prevented its degradation, and extension of this structure (green) resulted in a 114 nt unligatable extended product (unligatable extended S7).

Fig. S7.

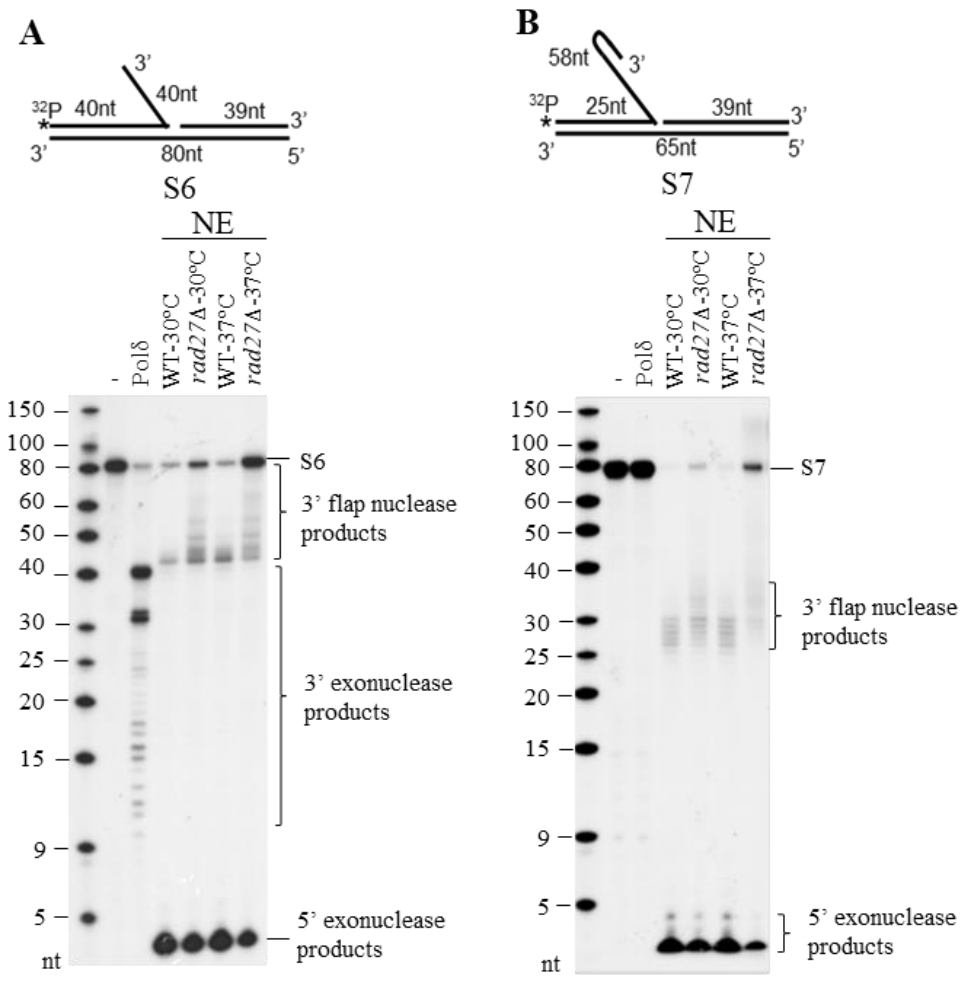

Fig. S7. 3' flap processing by nuclear extract (NE) from WT or *rad27*Δ yeast cells grown at 30°C or 37°C. The 3' flap substrate S6 **(A)** or the fold-back forming 3' flap substrate S7 **(B)** was incubated with purified recombinant Polδ (100 ng) or NE (1 μg each reaction) from the indicated yeast cell culture at 37°C for 15 min. Substrates and products were analyzed using 15% denaturing PAGE.

Fig. S8.

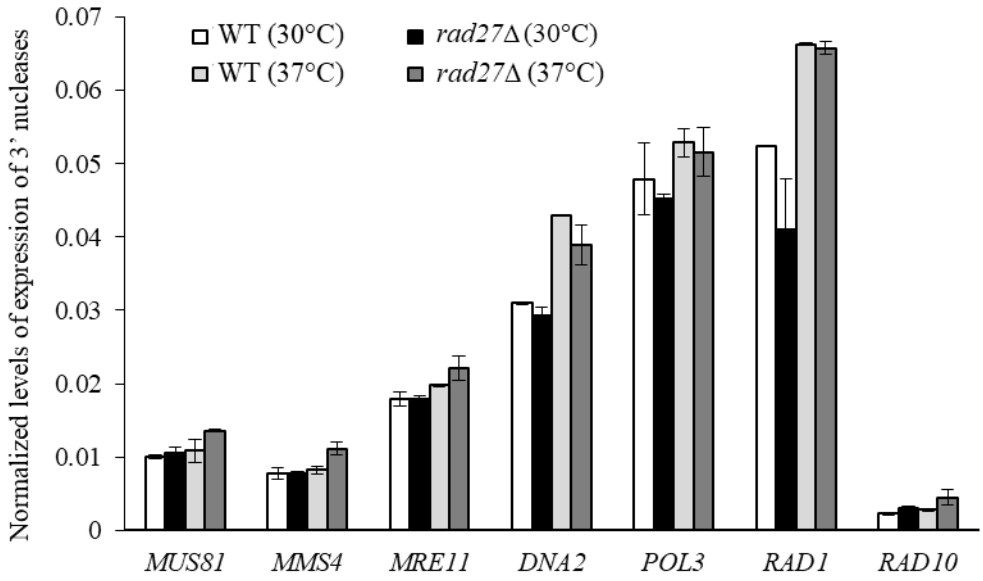

Fig. S8. Relative gene expression levels of representative 3' nucleases in WT or *rad27*Δ cells. Gene expression profiling of WT or *rad27*Δ cells grown at 30℃ or 37℃ was conducted using RNA-seq. The relative expression levels were calculated by normalizing the fragments per kilobase of transcript per million mapped reads (FPKM) of a specific gene with the FPKM of ACT1 in a sample. Values shown are averages of two biological replicates. Error bars indicate s.d.

Fig. S9.

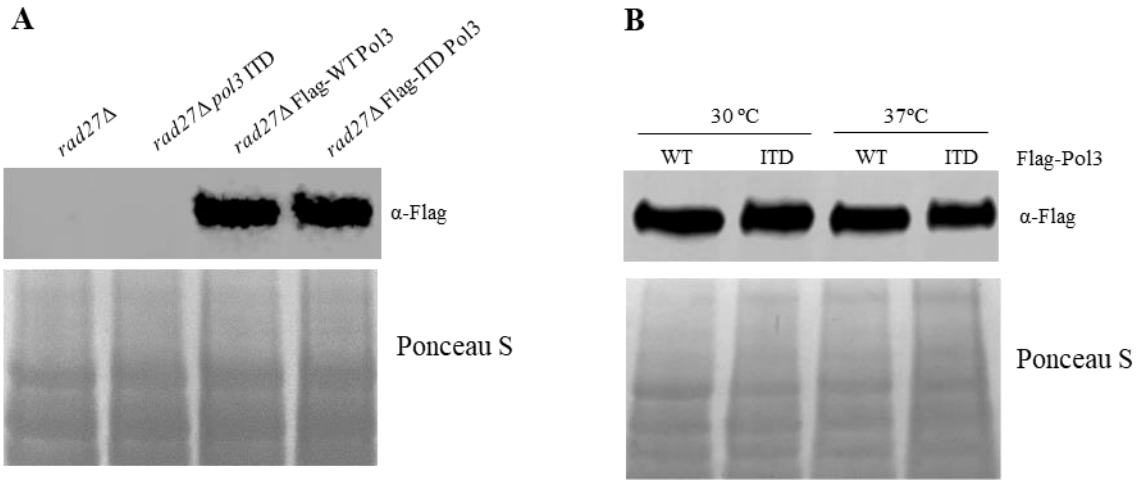

Fig. S9. Levels of WT Pol3 and ITD Pol3 at 30ºC or 37ºC. A DNA fragment encoding a flag tag was knocked into *rad27*Δ yeast cell bearing a WT *POL3* or *pol3* ITD gene, to express Flag-tagged WT Pol3 (Flag-Pol3) or Flag-tagged Pol3 ITD (Flag-ITD). **(A)** Western blot verifying knock-in of the Flag tag-encoding sequence at the WT *POL3* or *pol3* ITD gene in the *rad27*Δ strain using anti-Flag antibody. **(B)** Western blot for protein expression of Flag-tagged WT Pol3 (WT) and ITD Pol3 (ITD) in *rad27*Δ cells at 30ºC or 37ºC using anti-Flag antibody. Ponceau S staining of total proteins was used as a loading control in both panels.

Fig. S10.

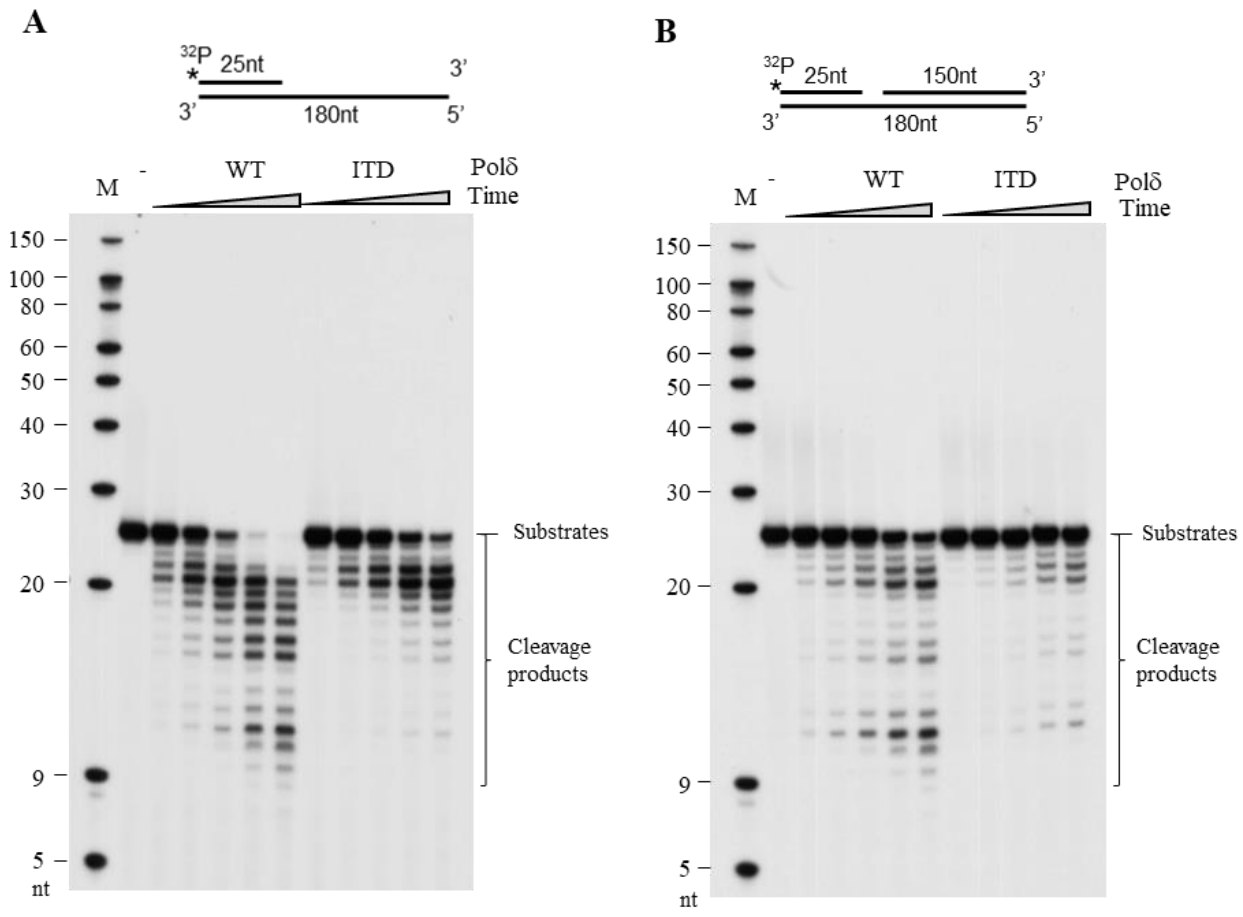

Fig. S10. Nuclease activity of WT Polδ and Polδ-ITD. Recombinant WT Polδ or Polδ-ITD protein (20 nM) was incubated with ^{32}P-labeled DNA substrates (100 nM, top panels) that were identical to the substrates for primer extension (panel A) and displacement DNA synthesis (panel B) assays (Tables S5, S6). The reactions were carried out at 30°C for 2.5, 5, 10, 20, 40 min and analyzed using 15% denaturing PAGE.

Fig. S11.

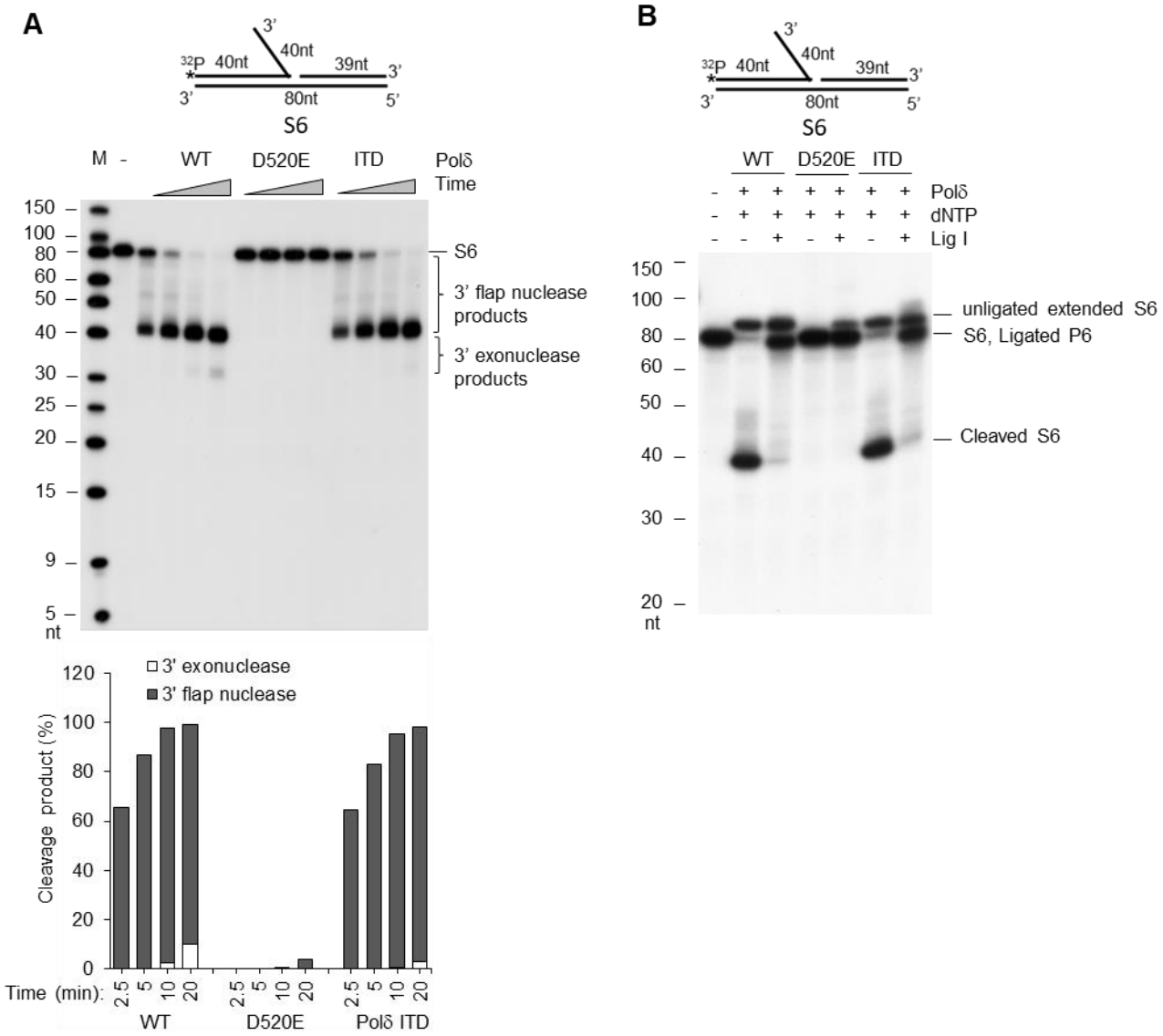

Fig. S11. 3' flap processing and 3' flap-based OFM by recombinant WT Polδ, nuclease-dead Polδ D520E, and Polδ-ITD. (A) 3' flap cleavage and subsequent 3' exonuclease cleavage of ^{32}P-labeled 3' flap DNA substrate by WT Polδ, nuclease-dead Polδ D520E, and Polδ-ITD. Top, diagram of ^{32}P-labeled substrate with a 40 nt 3' flap (S6) (Tables S5, S6). Middle, representative PAGE image of the nuclease activity assay. The substrate and cleavage products are indicated. Bottom, quantification of the 3' flap nuclease and subsequent exonuclease cleavage products. **(B)** Reconstituted 3' flap-based OFM by WT Polδ, nuclease-dead Polδ D520E, and Polδ-ITD. Top, diagram of ^{32}P-labeled substrate S6. Bottom, representative PAGE image of the nuclease activity assay. The substrate (S6), cleavage product (cleaved S6), unligated extended product (unligated extended S6), and ligated product (P6) are indicted.

Fig. S12.

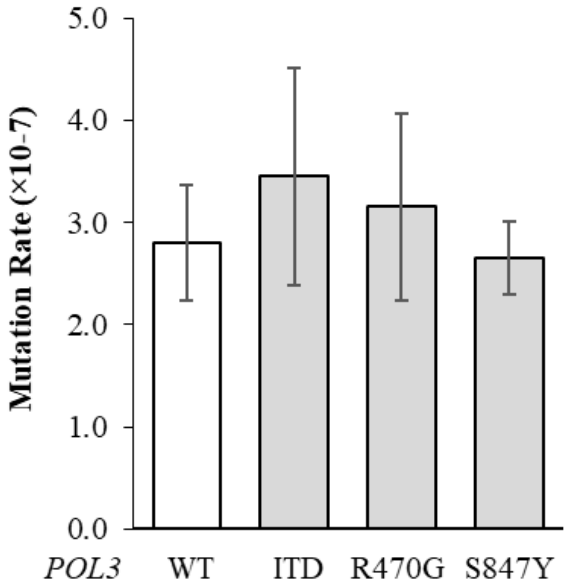

Fig. S12. No significant differences in the mutation rate of the WT yeast strain or mutant yeast strains carrying *pol3* knock-in mutations. Three representative *pol3* mutations (*pol3* ITD, R470G, or S847Y) were introduced into the *POL3* allele. Mutation rates of the WT and knock-in mutant yeast strains were determined using Can^r mutation assay. Values shown are means ± s.d. of three independent assays.

Fig. S13.

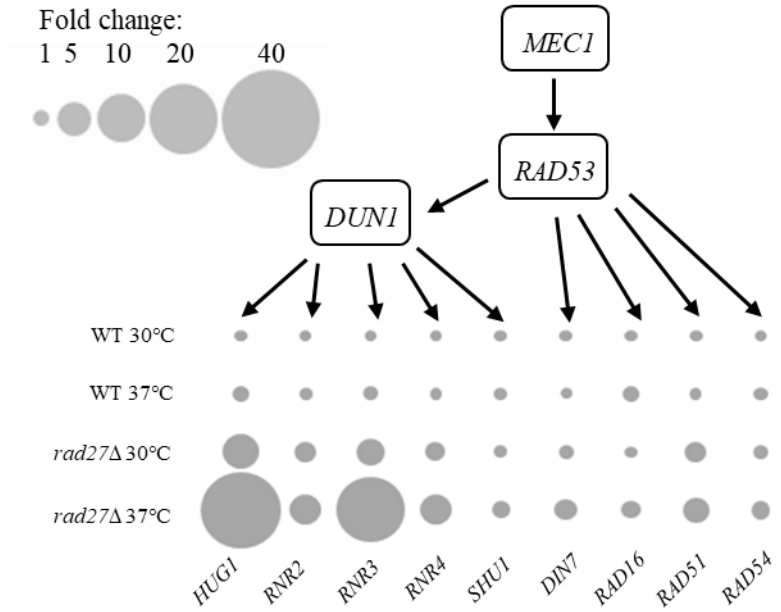

Fig. S13. Diagram of fold-changes in gene expression levels of DNA damage response and repair genes that are mediated by the Mec1-Rad53-Dun1 axis. Gene expression profiling of WT or *rad27*Δ cells grown at 30℃ or 37℃ was determined using RNA-seq. Fold-changes were calculated by comparing the normalized fragments per kilobase of transcript per million mapped reads (FPKM) of a specific gene in a sample with the normalized FPKM of the same gene in the control (WT, 30℃), which was arbitrarily set as 1.

Fig. S14.

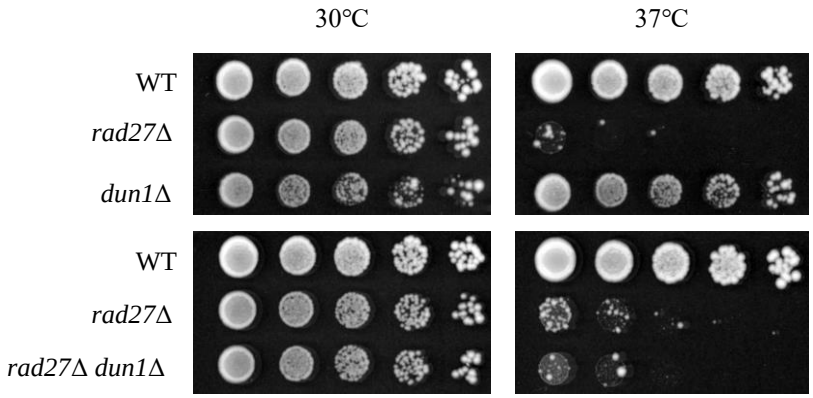

Fig. S14. *DUN1* knockout has little effect on the viability of *rad27*Δ cells. Viability of WT, *rad27*Δ, *dun1*Δ, or *rad27*Δ *dun1*Δ cells was analyzed using spot assays. Yeast cells of the indicated genetic backgrounds were serially diluted, spotted on YPD plates, and incubated at 30°C or 37°C for 48 h.

Fig. S15.

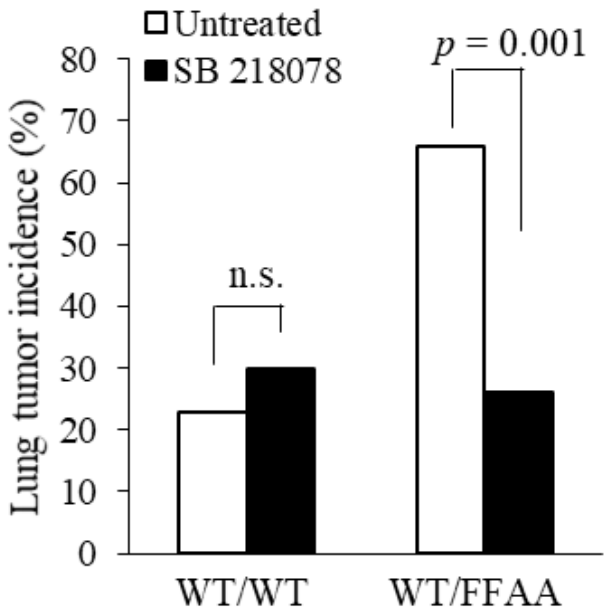

Fig. S15. Chk1 inhibition blocks lung cancer development in FEN1 mutant mice. WT (*n*=23) and WT/F343AF344A (WT/FFAA) (*n*=38) mice were treated with the Chk1 inhibitor SB218078 (0.025 mg/kg body weight). In the untreated control groups, WT (*n*=31) and WT/FFAA (*n*=35) were administered DMSO. p value was calculated by the Fisher Exact test.

Fig. S16.

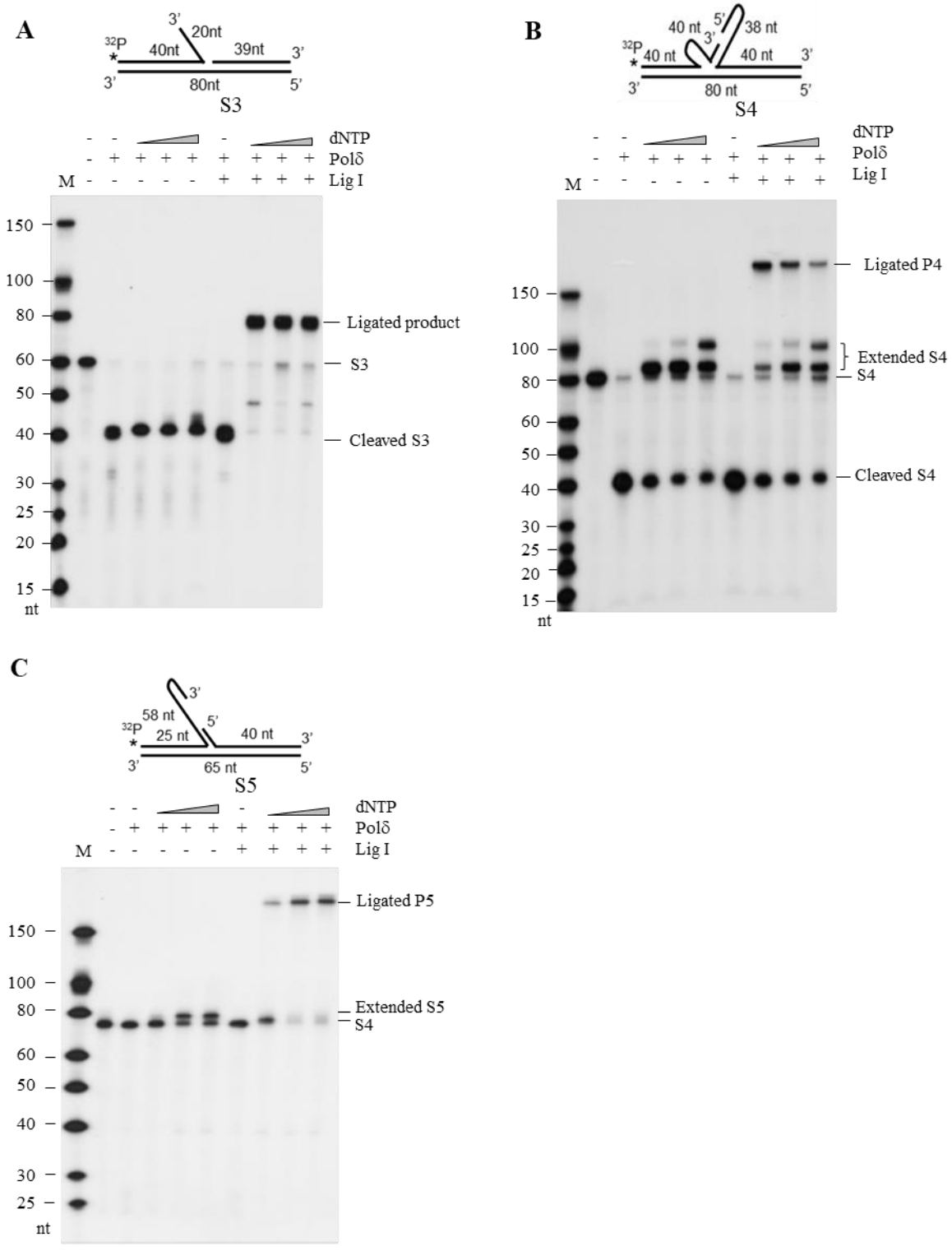
A
3'
20nt
32P
40nt
39nt
3'
3'
80nt
5'
S3
dNTP
Polδ
Lig I
M
150
100
80
60
50
40
30
25
20
15
nt
Ligated product
S3
Cleaved S3
B
40 nt
5'
38 nt
3'
32P
40 nt
40 nt
3'
3'
80 nt
5'
S4
dNTP
Polδ
Lig I
M
Ligated P4
Extended S4
S4
Cleaved S4
C
3'
58 nt
5'
32P
25 nt
40 nt
3'
3'
65 nt
5'
S5
dNTP
Polδ
Lig I
M
Ligated P5
Extended S5
S4

Fig. S16. Impact of deoxyribonucleotides (dNTP) on 3' flap-based OFM. Reconstituted 3' flap-based OFM by WT Polδ in the presence of varying concentrations of dNTP (10 μM, 100 μM, and 1 mM) using **(A)** ^{32}P-labeled 3' flap substrate S3 and ^{32}P-labeled secondary structure-forming 3' flap substrate **(B)** S4 or **(C)** S5. Reactions were carried out at 37°C and analyzed using 8% denaturing PAGE. The substrates (S3, S4, S5), cleavage products (Cleaved S3, S4), extended intermediates (Extended S3, S4, S5), and ligated product (Ligated P3, P4, P5) are indicted.

Fig. S17.

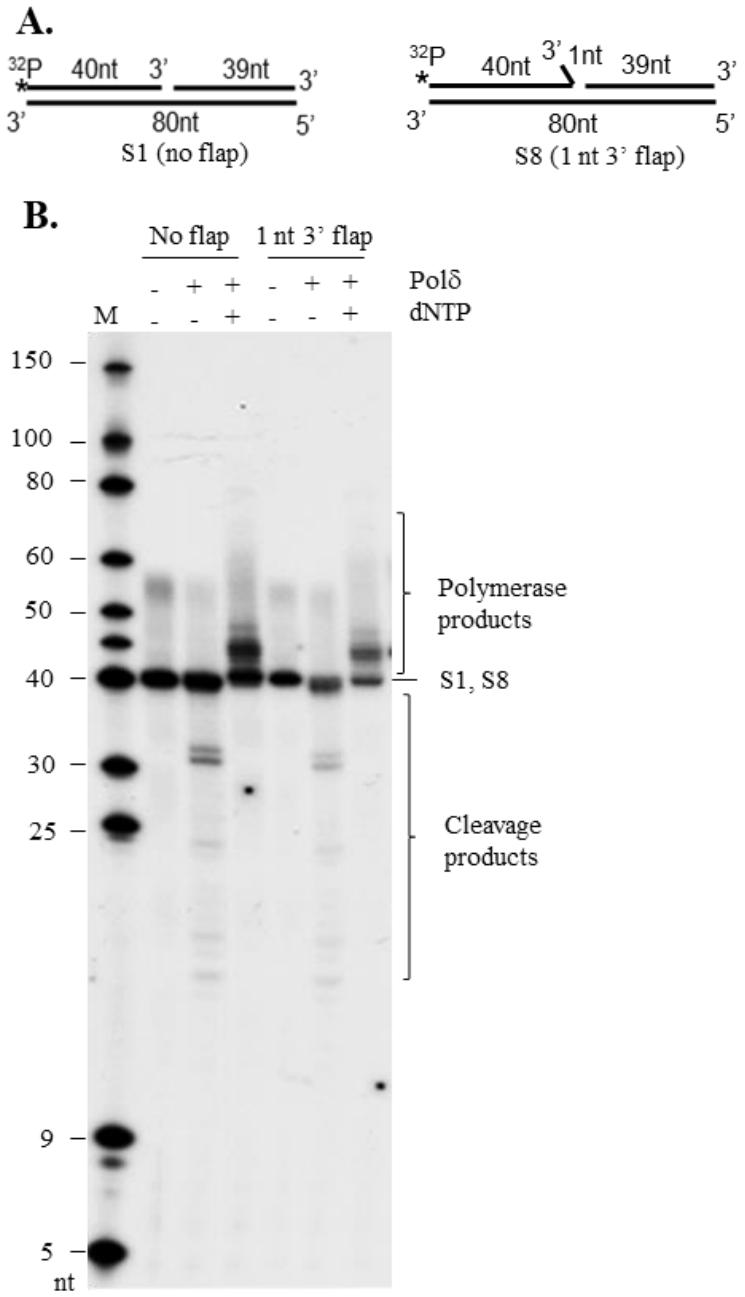

Fig. S17. Nuclease activity of Polδ on a gapped duplex with or without a 1 nt 3' flap. (A) Gapped DNA duplex substrate with or without a 1 nt 3' flap (Table S5). **(B)** WT Polδ (5 nM) was incubated with ^{32}P-labeled DNA substrates (100 nM). The reactions were carried out at 30°C for 20 min and analyzed using 15% denaturing PAGE.

Fig. S18.

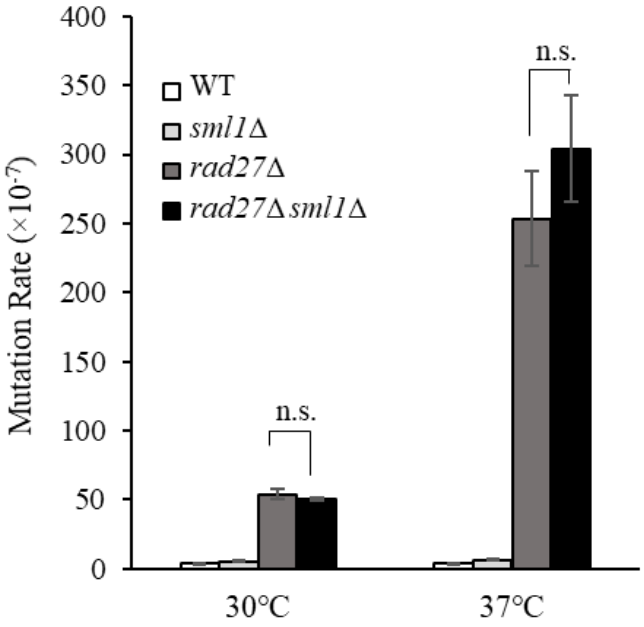

Fig. S18. *SML1* deletion has little effect on the mutation rate of the WT yeast strain or the *rad27*Δ yeast strain. The mutation rates of WT and *rad27*Δ cells at 30℃ or 37℃ were determined using a Can^r mutation assay. Values shown are means ± s.d. of three independent assays. p value was calculated using Student's t test. n.s., not significant.

Fig. S19.

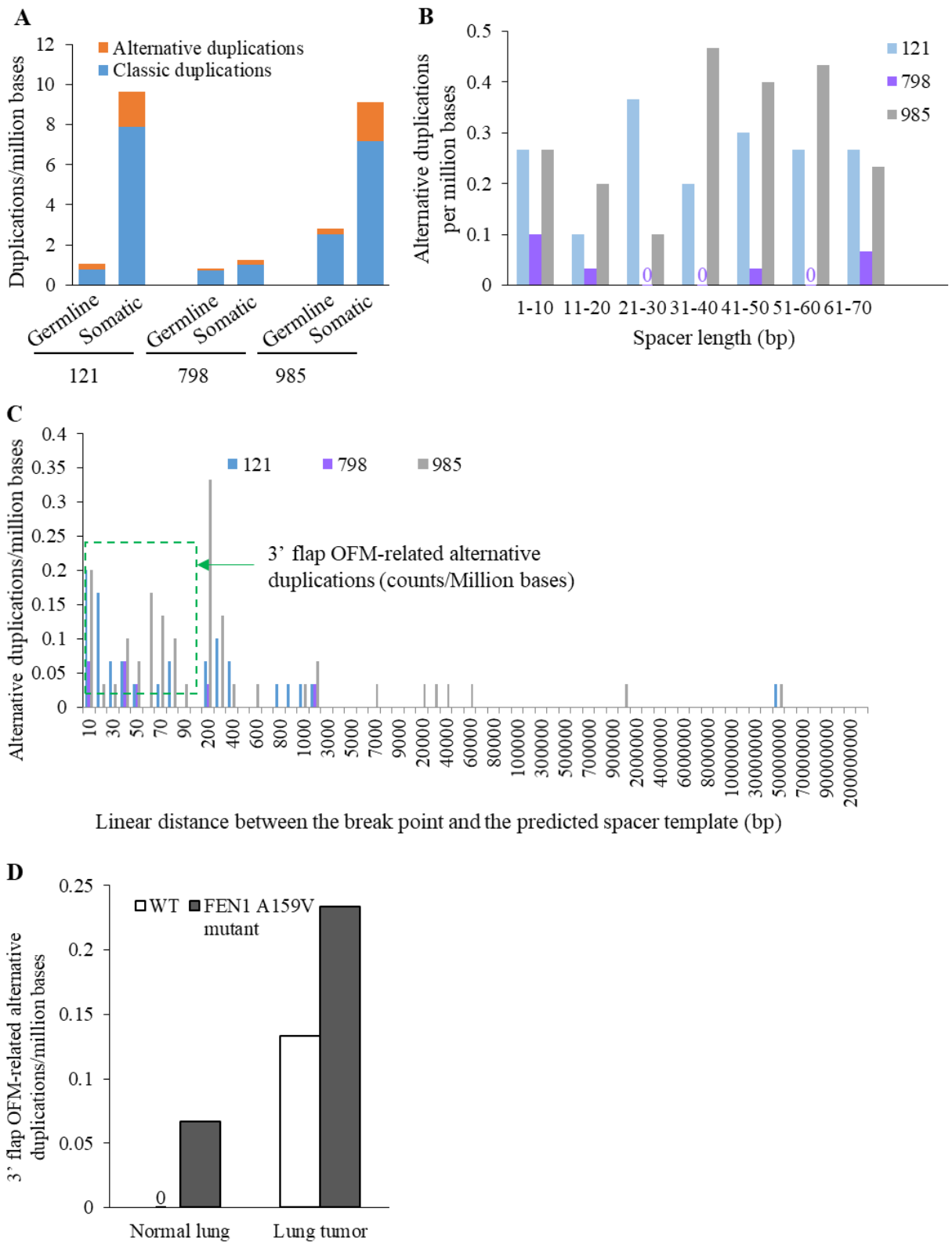
A
Alternative duplications
Classic duplications
Duplications/million bases
Germline
Somatic
121
798
985
B
121
798
985
Alternative duplications per million bases
1-10
11-20
21-30
31-40
41-50
51-60
61-70
Spacer length (bp)
C
121
798
985
3' flap OFM-related alternative duplications (counts/Million bases)
Alternative duplications/million bases
Linear distance between the break point and the predicted spacer template (bp)
D
WT
FEN1 A159V mutant
3' flap OFM-related alternative duplications/million bases
Normal lung
Lung tumor

Fig. S19. 3' flap OFM-related alternative duplications in human B cell acute lymphoblastic leukemia (ALL) and mouse lung tumors. (A)-(C) Germline and somatic duplications in three tumor specimens from randomly selected B cell ALL from the published datasets (41). The duplications present in both tumor and normal samples were considered germline, and those that were present in the tumor samples were considered somatic. **(A)** Frequency of germline and somatic classic and alternative duplications in the three ALL cancer specimens. Classic duplications were simple duplication mutations with no spacer and the alternative duplications were duplications with a spacer DNA sequence between the duplication units (See Fig. 2C for illustration). **(B)** The lengths of spacers in the alternative duplications in the three ALL specimens are shown. They ranged from 1 nt to 70 nt, which was similar to the spacer lengths for stress temperature-induced alternative duplications in *rad27*Δ. **(C)** Relative locations of donor DNA sequences that serve as the template for the intervening spacer DNA. The spacer DNA sequences were mapped across the human genome. For alternative duplications whose duplication unit and the donor DNA sequences for the spacer DNA were on the same chromosome, the linear distance between the duplication unit (break point) and the corresponding spacer donor sequence was calculated. The green boxed portion shows those 3' flap OFM-related alternative duplications. **(D)** Somatic 3' flap OFM-related alternative duplications in WT and FEN1 A159V/WT mutant mice. Somatic 3' flap OFM-related alternative duplications in WT or A159V/WT normal lung or lung tumor (n=1 for each sample) were identified. 3' flap OFM-related alternative duplications that were only present in the normal lung or lung tumor samples were considered somatic.

Fig. S20.

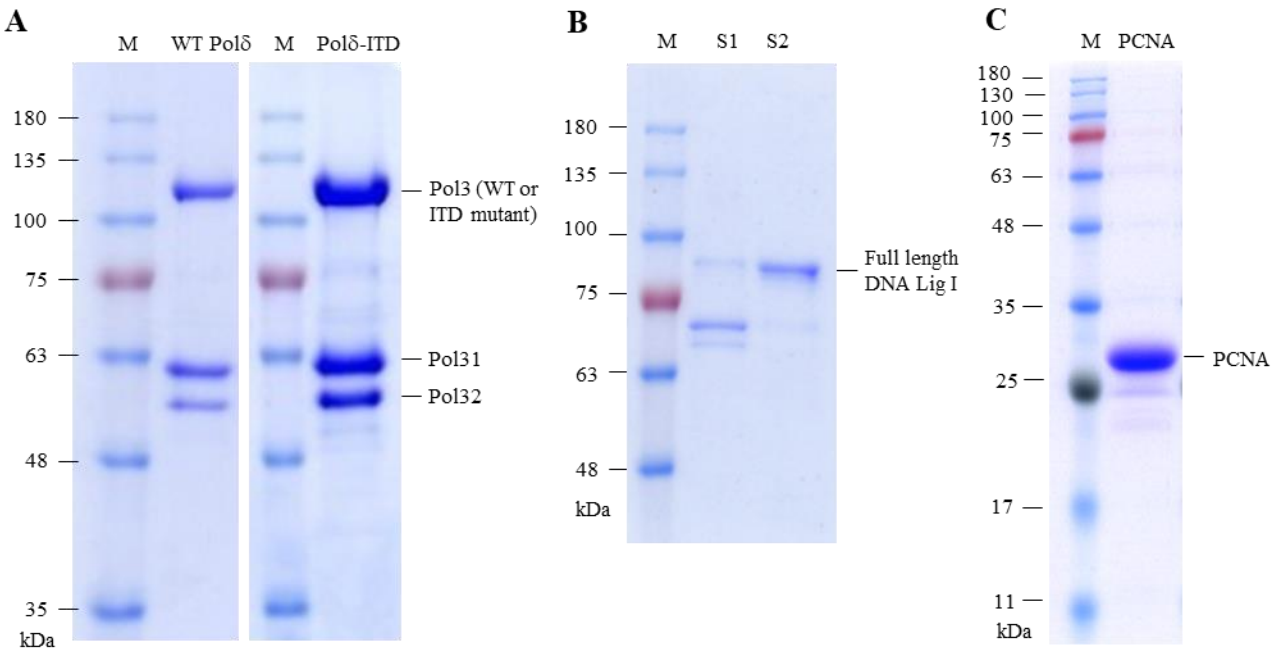

Fig. S20. SDS-PAGE of purified recombinant Polδ, DNA Lig I, and PCNA proteins. (A) Yeast WT Polδ and Polδ-ITD. Three subunits, Pol3 (WT or ITD), Pol31, and Pol32, of yeast Polδ were co-expressed in yeast and purified using chromatography as described in the Methods section. The purity of WT Polδ or Pol δ-ITD was evaluated by resolving proteins on 10% SDS-PAGE. **(B)** 6His-tagged DNA Lig I was expressed in *E. coli* and purified using chromatography as described in the Methods section. The purity of DNA Lig I was evaluated by resolving proteins using 10% SDS-PAGE. S1: the eluted peak fraction of Ni-NTA chromatography, S2: the eluted peak fraction of heparin chromatography. **(C)** 6His-tagged PCNA was expressed in *E. coli* and purified by chromatography as described in the Methods section. The purity of PCNA was evaluated by resolving the protein using 15% SDS-PAGE. All gels were stained with Coomassie blue 250. M: protein markers.

Table S1.

Table S1: Summary of enriched mutations in one *rad27*Δ revertant

Chromo.	Position	Reference	Variance in Revertant	Mutation Type*	*rad27*Δ(30°C)	*rad27*Δ Revertant	Genomic Region
chrIV	278279	C	G	SNP	0.0	100.0	YDL102W/POL3
chrXV	918461	G	T	SNP	0.0	100.0	Intergenic
chrIV	486317	A	-T	INDEL	0.0	50.0	YDR020C/DAS2
chrXII	547680	C	+AT	INDEL	0.0	33.3	Intergenic
chrVII	398468	C	+AT	INDEL	0.0	30.8	Intergenic
chrXI	80905	C	-T	INDEL	0.0	30.0	Intergenic
chrVIII	122057	G	+A	INDEL	0.0	22.7	Intergenic
chrXV	309087	T	+TA	INDEL	0.0	22.5	Intergenic
chrXV	998345	A	+AT	INDEL	0.0	20.0	Intergenic
chrVI	179312	T	+TTC	INDEL	0.0	20.0	YFR016C/AIP5
chrIX	195741	T	+GCATCCTTTAAAGAAGCA	INDEL	0.0	20.0	YIL089W
chrXII	75	A	T	SNP	1.0	97.1	Intergenic
chrVII	579015	G	+GGACATTGACGTACAATGGTTCA	INDEL	0.0	54.8	YGR041W/BUD9
chrVIII	560568	T	C	SNP	4.0	55.3	YHR219W
chrVIII	560579	A	C	SNP	0.0	82.5	YHR219W
chrI	205520	C	T	SNP	0.9	39.2	YAR050W/FLO1
chrXII	451538	C	A	SNP	2.3	76.1	Intergenic
chrXIV	415129	A	T	SNP	3.8	80.4	YNL112W/DBP2
chrXIII	88	T	C	SNP	1.9	83.1	Intergenic
chrXV	315630	C	A	SNP	2.6	74.5	Intergenic
chrVIII	560570	C	G	SNP	4.2	61.6	YHR219W

* SNP: Single Nucleotide Polymorphism; INDEL: Insertion/Deletion Polymorphism

Table S2.

Table S2: Viability test of *rad27Δ pol3* ITD *exo1Δ* cells via genetic crosses and random spore analysis

Genetic Cross	Colony No. (YPD Plates)[1]	Colony No. (SC Plates)[2]	Observed Ratio[3]	Expected Ratio[4]
pol3 ITD::*HIS3* x *exo1Δ::URA3*	2288	*pol3 ITD exo1Δ* 610	0.27	0.25
rad27Δ::LEU2 x *exo1Δ::URA3*	2865	*rad27Δ exo1Δ* 26	0.009	0.25
rad27Δ::LEU2 pol3 ITD::*HIS3* x *exo1Δ::URA3*	2788	*rad27Δ pol3* ITD *exo1Δ* 18	0.006	0.125

[1]Counted number of viable spores grown on YPD plates.

[2]Counted number of viable spores grown on nutrient-deficient synthetic complete (SC) medium plates. SC-His-Ura, SC-Leu-Ura, or SC-His-Leu-Ura were used for selection of *pol3 ITD exo1Δ, rad27 Δ exo1Δ, or rad27Δ pol3* ITD *exo1Δ* cells, respectively.

[3]Ratio of the viable spore number on the SC plates to the viable spore number on the YPD plates.

[4]Expected Mendelian ratio of spores with a specific allele combination based on the laws of segregation and independent assortment.

Table S3.

Table S3: Viability test of *rad27Δ pol3* ITD *dna2-1* cells via genetic crosses and DNA sequencing

Genetic Cross	Total Sequenced Colony No.[1]	Colony No. With the *dna2-1* Allele[2]	Observed Ratio[3]	Expected Ratio[4]
pol3 ITD::*HIS3* x *dna2-1*	*pol3* ITD 38	*pol3 ITD dna2-1* 18	0.47	0.5
rad27Δ::LEU2 x *dna2-1*	*rad27Δ* 40	*rad27Δ dna2-1* 0	0	0.5
rad27Δ::LEU2 pol3 ITD::*HIS3* x *dna2-1*	*rad27Δ pol3* ITD 60	*rad27Δ pol3* ITD *dna2-1* 0	0	0.5

[1]Counted number of viable spores that grew on nutrient-deficient SC medium plates and were sequenced for the *DNA2* gene. SC-His, SC-Leu, or SC-His-Leu SC plates were used for selection of *pol3 ITD, rad27Δ, or pol3 ITD rad27Δ* viable spores, respectively.

[2]Number of sequenced viable spores carrying the *dna2-1* allele.

[3]Ratio of the number of viable spores carrying the *dna2-1* allele to the total number of viable spores being sequenced.

[4]Expected Mendelian ratio of spores with the *dna2-1* allele based on the law of segregation.

Table S4.

Table S4: Yeast strains used in this work

strains	Mating type	Relevant genotype	Source
RDKY2672	a	WT	Richard D. Kolodner
RDKY2669	α	WT	Richard D. Kolodner
RDKY2608	a	*rad27*Δ::*URA3*	Richard D. Kolodner
YRP654-FLAG-POL3	a	p*POL3*-FLAG/*LEU2*	Satya Prakash
4×154-9A	a	*dna2-1* P504S	Judith L. Campbell
HTS-Y-30	a	*rad27*Δ::*LEU2*	This study
HTS-Y-3	a	*POL3*::*HIS3*	This study
HTS-Y-130	a	*pol3* ITD::*HIS3*	This study
HTS-Y-139	a	*pol3* R470G::*HIS3*	This study
HTS-Y-123	a	*pol3* S847Y::*HIS3*	This study
HTS-Y-15	a	*rad27*Δ::*URA3 pol3* ITD::*HIS3*	This study
HTS-Y-11	a	*rad27*Δ::*URA3 pol3* R470G::*HIS3*	This study
HTS-Y-12	a	*rad27*Δ::*URA3 pol3* R475I::*HIS3*	This study
HTS-Y-14	a	*rad27*Δ::*URA3 pol3* A484V::*HIS3*	This study
HTS-Y-16	a	*rad27*Δ::*URA3 pol3* S847Y::*HIS3*	This study
HTS-Y-50	a	*rad27* Δ::*LEU2 POL3*::*HIS3*	This study
HTS-Y-62	a	*rad27*Δ::*LEU2 pol3* ITD::*HIS3*	This study
HTS-Y-53	a	*rad27*Δ::*LEU2 pol3* R475I::*HIS3*	This study
HTS-Y-60	a	*rad27*Δ::*LEU2 pol3* S847Y::*HIS3*	This study
HTS-Y-40	a	p*POL3*-FLAG/*LEU2* p*POL31*/*POL32*-GST/*TRP1*	This study
HTS-Y-124	a	p*pol3* ITD-FLAG/ *LEU2* pPOL31/*POL32*-GST/*TRP1*	This study
HTS-Y-97	a	p*pol3* D520E-FLAG/ *LEU2* p*POL31*/*POL32*-GST/*TRP1*	This study
HTS-Y-148	a	*dun1*Δ::*HIS3*	This study
HTS-Y-173	a	*rad27*Δ::*URA3 dun1*Δ::*HIS3*	This study
HTS-Y-193	a	*sml1*Δ::*TRP1*	This study
HTS-Y-195	a	*rad27*Δ::*URA3 sml1*Δ::*TRP1*	This study
HTS-Y-199	a	*rad27*Δ::*URA3 POL3*-5FLAG::HphMx	This study
HTS-Y-201	a	*rad27*Δ::*URA3 pol3* ITD-5FLAG::HphMx::*HIS3*	This study
HTS-Y-202	α	*rad27*Δ::*LEU2*	This study
HTS-Y-203	α	*rad27*Δ::*LEU2 pol3* ITD::*HIS3*	This study
HTS-Y-204	α	*pol3* ITD::*HIS3*	This study
HTS-Y-205	α	*exo1*Δ::*URA3*	This study

Table S5.

Table S5: Oligos used for synthetic DNA substrates in this work*

Substrate	Upstream	Downstream	Template
S1	3FLAP0	D39	T80
S2	3FLAP10	D39	T80
S3	3FLAP20	D39	T80
S4	3FLAP40	5FLAPFB	T80
S5	3FLAPFB	D54	T65
S6	3FLAP40	D39	T80
S7	3FLAPFB	D39	T65
S8	3FLAP1	D39	T80
Primer extension	U25	-	T180
Displacement DNA synthesis	U25	D150	T180

*Oligo sequences are shown in Table S6

Table S6.

Table S6: Sequences of the oligos used for synthetic substrates in this work

Oligo Name	Oligo sequences
3FLAP0	5' GCTTAAGGACTCTGCCTCAACTCCACAGAGCTAGATTTCC 3'
3FLAP1	5' GCTTAAGGACTCTGCCTCAACTCCACAGAGCTAGATTTCCC 3'
3FLAP10	5' GCTTAAGGACTCTGCCTCAACTCCACAGAGCTAGATTTCCAGTGCACAAG 3'
3FLAP20	5' GCTTAAGGACTCTGCCTCAACTCCACAGAGCTAGATTTCCGCAACTGTGTGGATGTGACG 3'
3FLAP40	5' GCTTAAGGACTCTGCCTCAACTCCACAGAGCTAGATTTCCGCAACTGTGTGGATGTGACGATGGCGTAGCAGTGCACAAG 3'
3FLPFB	5' CCCATGGTTGTGGCGCCTTTGAATT CCATAGTAGATTCAAAGCCTACAATGCTGCAAGGACAAGCCCCGTCGGGGCTTGTCCT 3'
D39	5' GTTAGGACTGCTTGACATCCCAAGCAGACCTATCTTAAC 3'
D54	5' GAATCTACTATGGTTTTTAGGACTGCTTGACATCCCAAGCAGACCTATCTTAAC3'
5FLAPFB	5' CTGGCACTTCGGAGAAGTGCCAGTTTTCTTGTGCTTTTAGTTAGGACTGCTTGACATCCCAAGCAGACCTATCTTAAC 3'
T80	5' GTTAAGATAGGTCTGCTTGGGATGTCAAGCAGTCCTAACT GGAAATCTAGCTCTGTGGAGTTGAGGCAGAGTCCTTAAGC 3'
T65	5' GTTAAGATAGGTCTGCTTGGGATGTCAAGCAGTCCTAACTAATTCAAAGGCGCCACAACCATGGG 3'
U25	5' GCTTGACATCCCAAGCAGACCTATC 3'
D150	5'ATCAGGAAGTTCATATAAAAGGCAAACGGAAGCATTCTCAGAATATTCTTTGTGATGATGGAGTTTCACACACAGAGCTGAACATG CCTT TTGATGGAGCAGTTTCCAAATACACTTTTGGTAGAATCTGCAGGTGGATATTGATGGGGG3'
T180	5'CCCCCATCAATATCCACCTGCAGATTCTACCAAAAGTGTATTTGGAAACTGCTCCATCAAAAGGCATGTTCAGCTCTGTGTGTGAA ACTCCATCATCACAAAGAATATTCTGAGAATGCTTCCGTTTGCCTTTTATATGAACTTCCTGATGTTAAGATAGGTCTGCTTGGGATG TCAAGC 3'

References and Notes

1. D. M. Fitzgerald, P. J. Hastings, S. M. Rosenberg, Stress-induced mutagenesis: Implications in cancer and drug resistance. *Annu. Rev. Cancer Biol.* **1**, 119–140 (2017). doi:10.1146/annurev-cancerbio-050216-121919 Medline

2. R. S. Galhardo, P. J. Hastings, S. M. Rosenberg, Mutation as a stress response and the regulation of evolvability. *Crit. Rev. Biochem. Mol. Biol.* **42**, 399–435 (2007). doi:10.1080/10409230701648502 Medline

3. T. Ogawa, T. Okazaki, Discontinuous DNA replication. *Annu. Rev. Biochem.* **49**, 421–457 (1980). doi:10.1146/annurev.bi.49.070180.002225 Medline

4. P. M. J. Burgers, T. A. Kunkel, Eukaryotic DNA replication fork. *Annu. Rev. Biochem.* **86**, 417–438 (2017). doi:10.1146/annurev-biochem-061516-044709 Medline

5. S. A. Nick McElhinny, D. A. Gordenin, C. M. Stith, P. M. Burgers, T. A. Kunkel, Division of labor at the eukaryotic replication fork. *Mol. Cell* **30**, 137–144 (2008). doi:10.1016/j.molcel.2008.02.022 Medline

6. S. Waga, B. Stillman, Anatomy of a DNA replication fork revealed by reconstitution of SV40 DNA replication in vitro. *Nature* **369**, 207–212 (1994). doi:10.1038/369207a0 Medline

7. M. R. Lieber, The FEN-1 family of structure-specific nucleases in eukaryotic DNA replication, recombination and repair. *BioEssays* **19**, 233–240 (1997). doi:10.1002/bies.950190309 Medline

8. S. H. Bae, K. H. Bae, J. A. Kim, Y. S. Seo, RPA governs endonuclease switching during processing of Okazaki fragments in eukaryotes. *Nature* **412**, 456–461 (2001). doi:10.1038/35086609 Medline

9. Y. Liu, H. I. Kao, R. A. Bambara, Flap endonuclease 1: A central component of DNA metabolism. *Annu. Rev. Biochem.* **73**, 589–615 (2004). doi:10.1146/annurev.biochem.73.012803.092453 Medline

10. M. S. Reagan, C. Pittenger, W. Siede, E. C. Friedberg, Characterization of a mutant strain of *Saccharomyces cerevisiae* with a deletion of the *RAD27* gene, a structural homolog of the *RAD2* nucleotide excision repair gene. *J. Bacteriol.* **177**, 364–371 (1995). doi:10.1128/jb.177.2.364-371.1995 Medline

11. K. C. Sitney, M. E. Budd, J. L. Campbell, DNA polymerase III, a second essential DNA polymerase, is encoded by the *S. cerevisiae CDC2* gene. *Cell* **56**, 599–605 (1989). doi:10.1016/0092-8674(89)90582-5 Medline

12. D. X. Tishkoff, N. Filosi, G. M. Gaida, R. D. Kolodner, A novel mutation avoidance mechanism dependent on *S. cerevisiae RAD27* is distinct from DNA mismatch repair. *Cell* **88**, 253–263 (1997). doi:10.1016/S0092-8674(00)81846-2 Medline

13. A. Mariño-Enriquez, A. Lauria, J. Przybyl, T. L. Ng, M. Kowalewska, M. Debiec-Rychter, R. Ganesan, V. Sumathi, S. George, W. G. McCluggage, M. R. Nucci, C.-H. Lee, J. A. Fletcher, BCOR internal tandem duplication in high-grade uterine sarcomas. *Am. J. Surg. Pathol.* **42**, 335–341 (2018). doi:10.1097/PAS.0000000000000993 Medline

14. P. D. Kottaridis, R. E. Gale, M. E. Frew, G. Harrison, S. E. Langabeer, A. A. Belton, H. Walker, K. Wheatley, D. T. Bowen, A. K. Burnett, A. H. Goldstone, D. C. Linch, The presence of a FLT3 internal tandem duplication in patients with acute myeloid leukemia (AML) adds important prognostic information to cytogenetic risk group and response to the first cycle of chemotherapy: Analysis of 854 patients from the United Kingdom Medical Research Council AML 10 and 12 trials. *Blood* **98**, 1752–1759 (2001). doi:10.1182/blood.V98.6.1752 Medline

15. H. Kiyoi, M. Towatari, S. Yokota, M. Hamaguchi, R. Ohno, H. Saito, T. Naoe, Internal tandem duplication of the *FLT3* gene is a novel modality of elongation mutation which causes constitutive activation of the product. *Leukemia* **12**, 1333–1337 (1998). doi:10.1038/sj.leu.2401130 Medline

16. Y. H. Jin, R. Ayyagari, M. A. Resnick, D. A. Gordenin, P. M. Burgers, Okazaki fragment maturation in yeast. II. Cooperation between the polymerase and 3′-5′-exonuclease activities of Pol δ in the creation of a ligatable nick. *J. Biol. Chem.* **278**, 1626–1633 (2003). doi:10.1074/jbc.M209803200 Medline

17. Z. Zhou, S. J. Elledge, *DUN1* encodes a protein kinase that controls the DNA damage response in yeast. *Cell* **75**, 1119–1127 (1993). doi:10.1016/0092-8674(93)90321-G Medline

18. X. Zhao, R. Rothstein, The Dun1 checkpoint kinase phosphorylates and regulates the ribonucleotide reductase inhibitor Sml1. *Proc. Natl. Acad. Sci. U.S.A.* **99**, 3746–3751 (2002). doi:10.1073/pnas.062502299 Medline

19. A. Chabes, V. Domkin, L. Thelander, Yeast Sml1, a protein inhibitor of ribonucleotide reductase. *J. Biol. Chem.* **274**, 36679–36683 (1999). doi:10.1074/jbc.274.51.36679 Medline

20. L. Zheng, H. Dai, M. Zhou, M. Li, P. Singh, J. Qiu, W. Tsark, Q. Huang, K. Kernstine, X. Zhang, D. Lin, B. Shen, Fen1 mutations result in autoimmunity, chronic inflammation and cancers. *Nat. Med.* **13**, 812–819 (2007). doi:10.1038/nm1599 Medline

21. S. H. Bae, Y. S. Seo, Characterization of the enzymatic properties of the yeast Dna2 helicase/endonuclease suggests a new model for Okazaki fragment processing. *J. Biol. Chem.* **275**, 38022–38031 (2000). doi:10.1074/jbc.M006513200 Medline

22. P. T. Tran, N. Erdeniz, S. Dudley, R. M. Liskay, Characterization of nuclease-dependent functions of Exo1p in *Saccharomyces cerevisiae*. *DNA Repair* **1**, 895–912 (2002). doi:10.1016/S1568-7864(02)00114-3 Medline

23. Y. H. Jin, R. Obert, P. M. Burgers, T. A. Kunkel, M. A. Resnick, D. A. Gordenin, The 3′→5′ exonuclease of DNA polymerase delta can substitute for the 5′ flap endonuclease Rad27/Fen1 in processing Okazaki fragments and preventing genome instability. *Proc. Natl. Acad. Sci. U.S.A.* **98**, 5122–5127 (2001). doi:10.1073/pnas.091095198 Medline

24. Y. Liu, H. Zhang, J. Veeraraghavan, R. A. Bambara, C. H. Freudenreich, *Saccharomyces cerevisiae* flap endonuclease 1 uses flap equilibration to maintain triplet repeat stability. *Mol. Cell. Biol.* **24**, 4049–4064 (2004). doi:10.1128/MCB.24.9.4049-4064.2004 Medline

25. A. Toulmay, R. Schneiter, A two-step method for the introduction of single or multiple defined point mutations into the genome of *Saccharomyces cerevisiae*. *Yeast* **23**, 825–831 (2006). doi:10.1002/yea.1397 Medline

26. M. E. Budd, J. L. Campbell, A yeast replicative helicase, Dna2 helicase, interacts with yeast FEN-1 nuclease in carrying out its essential function. *Mol. Cell. Biol.* **17**, 2136–2142 (1997). doi:10.1128/MCB.17.4.2136 Medline

27. D. X. Tishkoff, A. L. Boerger, P. Bertrand, N. Filosi, G. M. Gaida, M. F. Kane, R. D. Kolodner, Identification and characterization of *Saccharomyces cerevisiae EXO1*, a gene encoding an exonuclease that interacts with MSH2. *Proc. Natl. Acad. Sci. U.S.A.* **94**, 7487–7492 (1997). doi:10.1073/pnas.94.14.7487 Medline

28. A. E. Coluccio, R. K. Rodriguez, M. J. Kernan, A. M. Neiman, The yeast spore wall enables spores to survive passage through the digestive tract of Drosophila. *PLOS ONE* **3**, e2873 (2008). doi:10.1371/journal.pone.0002873 Medline

29. D. A. Treco, F. Winston, Growth and manipulation of yeast. *Curr. Protoc. Mol. Biol.* **82**, 13.2.1–13.2.12 (2008). doi:10.1002/0471142727.mb1302s82

30. R. A. Reenan, R. D. Kolodner, Characterization of insertion mutations in the *Saccharomyces cerevisiae MSH1* and *MSH2* genes: Evidence for separate mitochondrial and nuclear functions. *Genetics* **132**, 975–985 (1992). doi:10.1093/genetics/132.4.975 Medline

31. D. E. Lea, C. A. Coulson, The distribution of the numbers of mutants in bacterial populations. *J. Genet.* **49**, 264–285 (1949). doi:10.1007/BF02986080 Medline

32. L. Zheng, H. Dai, M. L. Hegde, M. Zhou, Z. Guo, X. Wu, J. Wu, L. Su, X. Zhong, S. Mitra, Q. Huang, K. H. Kernstine, G. P. Pfeifer, B. Shen, Fen1 mutations that specifically disrupt its interaction with PCNA cause aneuploidy-associated cancer. *Cell Res.* **21**, 1052–1067 (2011). doi:10.1038/cr.2011.35 Medline

33. S. Liu, G. Lu, S. Ali, W. Liu, L. Zheng, H. Dai, H. Li, H. Xu, Y. Hua, Y. Zhou, J. Ortega, G. M. Li, T. A. Kunkel, B. Shen, Okazaki fragment maturation involves α-segment error editing by the mammalian FEN1/MutSα functional complex. *EMBO J.* **34**, 1829–1843 (2015). doi:10.15252/embj.201489865 Medline

34. R. E. Johnson, L. Prakash, S. Prakash, Pol31 and Pol32 subunits of yeast DNA polymerase δ are also essential subunits of DNA polymerase ζ. *Proc. Natl. Acad. Sci. U.S.A.* **109**, 12455–12460 (2012). doi:10.1073/pnas.1206052109 Medline

35. R. E. Johnson, L. Prakash, S. Prakash, Yeast and human translesion DNA synthesis polymerases: Expression, purification, and biochemical characterization. *Methods Enzymol.* **408**, 390–407 (2006). doi:10.1016/S0076-6879(06)08024-4 Medline

36. P. M. Burgers, K. J. Gerik, Structure and processivity of two forms of *Saccharomyces cerevisiae* DNA polymerase δ. *J. Biol. Chem.* **273**, 19756–19762 (1998). doi:10.1074/jbc.273.31.19756 Medline

37. L. Zheng, M. Li, J. Shan, R. Krishnamoorthi, B. Shen, Distinct roles of two Mg^{2+} binding sites in regulation of murine flap endonuclease-1 activities. *Biochemistry* **41**, 10323–10331 (2002). doi:10.1021/bi025841s Medline

38. L. Zheng, M. Zhou, Z. Guo, H. Lu, L. Qian, H. Dai, J. Qiu, E. Yakubovskaya, D. F. Bogenhagen, B. Demple, B. Shen, Human DNA2 is a mitochondrial nuclease/helicase for efficient processing of DNA replication and repair intermediates. *Mol. Cell* **32**, 325–336 (2008). doi:10.1016/j.molcel.2008.09.024 Medline

39. Y. Quan, Y. Xia, L. Liu, J. Cui, Z. Li, Q. Cao, X. S. Chen, J. L. Campbell, H. Lou, Cell-cycle-regulated interaction between Mcm10 and double hexameric Mcm2-7 is required for helicase splitting and activation during S phase. *Cell Rep.* **13**, 2576–2586 (2015). doi:10.1016/j.celrep.2015.11.018 Medline

40. B. Cao, X. Wu, J. Zhou, H. Wu, L. Liu, Q. Zhang, M. S. DeMott, C. Gu, L. Wang, D. You, P. C. Dedon, Nick-seq for single-nucleotide resolution genomic maps of DNA modifications and damage. *Nucleic Acids Res.* **48**, 6715–6725 (2020). doi:10.1093/nar/gkaa473 Medline

41. A. M. Sriramachandran, G. Petrosino, M. Méndez-Lago, A. J. Schäfer, L. S. Batista-Nascimento, N. Zilio, H. D. Ulrich, Genome-wide nucleotide-resolution mapping of DNA replication patterns, single-strand breaks, and lesions by GLOE-Seq. *Mol. Cell* **78**, 975–985.e7 (2020). doi:10.1016/j.molcel.2020.03.027 Medline

42. M. D. Robinson, D. J. McCarthy, G. K. Smyth, edgeR: A Bioconductor package for differential expression analysis of digital gene expression data. *Bioinformatics* **26**, 139–140 (2010). doi:10.1093/bioinformatics/btp616 Medline

43. E. J. Jaehnig, D. Kuo, H. Hombauer, T. G. Ideker, R. D. Kolodner, Checkpoint kinases regulate a global network of transcription factors in response to DNA damage. *Cell Rep.* **4**, 174–188 (2013). doi:10.1016/j.celrep.2013.05.041 Medline

44. S. Falcon, R. Gentleman, Using GOstats to test gene lists for GO term association. *Bioinformatics* **23**, 257–258 (2007). doi:10.1093/bioinformatics/btl567 Medline

45. D. C. Koboldt, K. Chen, T. Wylie, D. E. Larson, M. D. McLellan, E. R. Mardis, G. M. Weinstock, R. K. Wilson, L. Ding, VarScan: Variant detection in massively parallel sequencing of individual and pooled samples. *Bioinformatics* **25**, 2283–2285 (2009). doi:10.1093/bioinformatics/btp373 Medline

46. K. Ye, M. H. Schulz, Q. Long, R. Apweiler, Z. Ning, Pindel: A pattern growth approach to detect break points of large deletions and medium sized insertions from paired-end short reads. *Bioinformatics* **25**, 2865–2871 (2009). doi:10.1093/bioinformatics/btp394 Medline

47. Z. Gu, M. L. Churchman, K. G. Roberts, I. Moore, X. Zhou, J. Nakitandwe, K. Hagiwara, S. Pelletier, S. Gingras, H. Berns, D. Payne-Turner, A. Hill, I. Iacobucci, L. Shi, S. Pounds, C. Cheng, D. Pei, C. Qu, S. Newman, M. Devidas, Y. Dai, S. C. Reshmi, J. Gastier-Foster, E. A. Raetz, M. J. Borowitz, B. L. Wood, W. L. Carroll, P. A. Zweidler-McKay, K. R. Rabin, L. A. Mattano, K. W. Maloney, A. Rambaldi, O. Spinelli, J. P. Radich, M. D. Minden, J. M. Rowe, S. Luger, M. R. Litzow, M. S. Tallman, J. Racevskis, Y. Zhang, R. Bhatia, J. Kohlschmidt, K. Mrózek, C. D. Bloomfield, W. Stock, S. Kornblau, H. M. Kantarjian, M. Konopleva, W. E. Evans, S. Jeha, C. H. Pui, J. Yang, E. Paietta, J. R. Downing, M. V. Relling, J. Zhang, M. L. Loh, S. P. Hunger, C. G. Mullighan, PAX5-driven subtypes of B-progenitor acute lymphoblastic leukemia. *Nat. Genet.* **51**, 296–307 (2019). doi:10.1038/s41588-018-0315-5 Medline

48. H. Fairfield, G. J. Gilbert, M. Barter, R. R. Corrigan, M. Curtain, Y. Ding, M. D'Ascenzo, D. J. Gerhardt, C. He, W. Huang, T. Richmond, L. Rowe, F. J. Probst, D. E. Bergstrom, S. A. Murray, C. Bult, J. Richardson, B. T. Kile, I. Gut, J. Hager, S. Sigurdsson, E. Mauceli, F. Di Palma, K. Lindblad-Toh, M. L. Cunningham, T. C. Cox, M. J. Justice, M. S. Spector, S. W. Lowe, T. Albert, L. R. Donahue, J. Jeddeloh, J. Shendure, L. G. Reinholdt, Mutation discovery in mice by whole exome sequencing. *Genome Biol.* **12**, R86 (2011). doi:10.1186/gb-2011-12-9-r86 Medline

49. W. J. Kent, BLAT—The BLAST-like alignment tool. *Genome Res.* **12**, 656–664 (2002). doi:10.1101/gr.229202 Medline

50. L. Zheng, J. Jia, L. D. Finger, Z. Guo, C. Zer, B. Shen, Functional regulation of FEN1 nuclease and its link to cancer. *Nucleic Acids Res.* **39**, 781–794 (2011). doi:10.1093/nar/gkq884 Medline

51. J. R. Jackson, A. Gilmartin, C. Imburgia, J. D. Winkler, L. A. Marshall, A. Roshak, An indolocarbazole inhibitor of human checkpoint kinase (Chk1) abrogates cell cycle arrest caused by DNA damage. *Cancer Res.* **60**, 566–572 (2000). Medline